Energy Reports 8 (2022) 13438–13462

Contents lists available at ScienceDirect

Energy Reports

journal homepage: www.elsevier.com/locate/egyr

Research paper

The techno-economic flexibility investigation and enhancement for the hybrid ocean-energy supported zero-energy building and seawater-transportation system

Xinman Guo [a], Haojie Luo [a], Sunliang Cao [a,d,e,*], Yixing Lisa Gao [b], Kai Pan [c]

[a] Renewable Energy Research Group (RERG), Department of Building Environment and Energy Engineering, Faculty of Construction and Environment, The Hong Kong Polytechnic University, Kowloon, Hong Kong Special Administrative Region
[b] School of Hotel and Tourism Management, The Hong Kong Polytechnic University, Kowloon, Hong Kong Special Administrative Region
[c] Department of Logistics and Maritime Studies, Faculty of Business, The Hong Kong Polytechnic University, Kowloon, Hong Kong Special Administrative Region
[d] Research Institute for Sustainable Urban Development (RISUD), The Hong Kong Polytechnic University, Kowloon, Hong Kong Special Administrative Region
[e] Research Institute for Smart Energy (RISE), The Hong Kong Polytechnic University, Kowloon, Hong Kong Special Administrative Region

ARTICLE INFO

Article history:
Received 23 May 2022
Received in revised form 24 September 2022
Accepted 28 September 2022
Available online 19 October 2022

Keywords:
Ocean renewable energy
Electric boat
Flexibility control
Zero-energy building
Coastal hotel building

ABSTRACT

Toward net zero emissions by 2050, efficient renewable energy systems and various energy interactions are increasingly proposed to improve energy matching and flexibility capacities. The existing studies primarily focused on onshore solar and wind energy sources, which can interact with electric vehicles or static batteries to improve the economic performance by the energy flexibility control. However, the hybrid system of ocean energy interacting with buildings and electric boats is rarely discussed. This study proposes an innovative integrated energy flexibility control to improve the techno-economic performance of a hybrid wave energy converter (WEC) and floating photovoltaic panel (FPV) energy system supporting a coastal hotel building and eight electric boats. We propose five control strategies, guaranteeing the normal excursion function of the boats while supporting enough energy for the building. In addition, two new indicators are presented to investigate the peak-shaving (PSI) and valley-filling (VFI) capabilities. A weighted matching index (WMI) is provided to investigate the overall energy matching capability. Annual electricity fees and relative net present value (NPV_{rel}) are introduced to analyse the economy. To analyse the environmental aspect, we use the annual operational equivalent CO_2 emissions (CE_a) to track the emissions of the hybrid system. We observe that strategy E, integrated with the non-dominated solutions from the other four strategies, shows a significant profitable economic performance The annual electricity fee is reduced by 12.22%, and the NPV_{rel} is improved by around 16.62%. PSI and VFI can reach 98.01% and 17.05% for a 100 kW line.

1. Introduction and background

1.1. Background

An increasing number of countries announce commitments to achieve net-zero emissions in the coming decades. As a major source of global emissions, the energy sector is key to meeting the climate challenge of the world (IEA, 2021b). As reported by International Energy Agency (IEA) (IEA, 2021b), the path to net-zero emissions by 2050 is still narrow unless all available clean energy technologies are massively deployed (including renewables, EVs, and energy-efficient building retrofits) throughout 2030. Indeed, renewables, zero-energy or -emission buildings, and various electric mobilities contribute to the global goal of reducing conventional fossil fuel consumption and CO_2 emissions in these years. In 2020, the share of increasing renewables in global electricity generation reached around 28.6%. However, if the 2050 net-zero emissions target is to be achieved, the proportion of electricity generated from renewables will need to reach 60% by 2030 (IEA, 2021d). Meanwhile, significant advances in energy efficiency over the past year have driven progress in decoupling energy consumption from floor space growth in the building sector (IEA, 2021e). For vehicles, despite the Covid-19 pandemic affecting public travel over the years, the electric

* Corresponding author at: Renewable Energy Research Group (RERG), Department of Building Environment and Energy Engineering, Faculty of Construction and Environment, The Hong Kong Polytechnic University, Kowloon, Hong Kong Special Administrative Region.
E-mail addresses: sunliang.cao@polyu.edu.hk, caosunliang@msn.com (S. Cao).

https://doi.org/10.1016/j.egyr.2022.09.185

Nomenclature

AHU	Air handling unit
CE_a	The annual operational equivalent CO_2 emission ($kgCO_{2,eq}/m^2.a$)
CEF_{eg}	The equivalent CO_2 emission factor of the electric grid ($kgCO_{2,eq}/kWh_e$)
CLP	China Light and Power Company Syndicate
C-rate	The rate at which a battery is being charged or discharged
$C_{EB,replacement,j}$	The total replacement cost of the boat batteries in year "j" (HKD)
$C_{imp,save,n}$	The saved electricity fee compared to the reference system (HKD)
$C_{subsidy,gen,n}$	The subsidy received for renewable energy generation (after inverter) during the year "n" (HKD)
DHW	Domestic hot water
E-Boat	Electric boat
$E_{exp,a}$	The annual export of electric energy to the grid (kWh/m^2. a)
$E_{imp,a}$	The annual import of electric energy from the grid ($kWh/m^2.a$)
FPV	Floating photovoltaic panel
FSOC	Fractional state of charge
I_{FPV}	The initial capital cost of the floating photovoltaic panel (HKD)
I_{WEC}	The initial capital cost of the wave energy converter (HKD)
L_{elec}	The total electrical demand power (kW)
$L_{EB_{sys}}$	The electric demand power of the electric boat for excursions (kW)
NPV_{rel}	Relative net present value (HKD)
OEFe	On-site electrical energy fraction
OEMe	On-site electrical energy matching
ORE	Ocean renewable energy
$P_{average,ref,p}$	The average imported power during the peak period of one year (kW)
$P_{average,ref,op}$	The average imported power during the off-peak period of one year (kW)
P_{dump}	The surplus power will be dumped (kW)
P_{EBpv}	The generation of power from the photovoltaic panels of the E-boat (kW)
P_{exp}	The power export to the grid (kW)
P_{imp}	The power import from the grid (kW)
$P_{j,p}$	The imported power of the Case $_j$ during the peak period (kW)
$P_{j,op}$	The imported power of the Case $_j$ during the off-peak period (kW)
P_{OREe}	The generation of power from ocean renewable energy systems (kW)
$P_{ref,p}$	The imported power of the reference case during the peak period (kW)
$P_{ref,op}$	The imported power of the reference case during the off-peak period (kW)
PSI	Peak shaving indicator
PV	Photovoltaic panel
REe	Renewable electricity
SV_{EB}	The salvage value of E-boat batteries (HKD)
VFI	Valley filling indicator
WEC	Wave energy converter
WMI	Weighted matching index
η_{EB}	The charging efficiency of the E-boat
p	Peak period
op	Off-peak period

vehicle market is still solid, and electric vehicles will become a more common sight on the roads of the world in the 2020s (IEA, 2021a,e). More efficient renewable energy systems and various energy interactions with electric vehicles have been proposed in the literature to enhance energy matching ability and flexibility.

1.2. Literature review

1.2.1. Building with renewables

There are two major technology solutions to the energy consumption problem in buildings: (i) use passive and active design to reduce self-energy consumption and (ii) apply on-site renewable energy systems to satisfy and enhance self-sufficiency. For example, a study by Lan et al. (2019) examined a holistic design approach to net-zero energy buildings for residents in Singapore. The study results showed that daylighting and natural cooling design contributed to energy efficiency and cost-effectiveness. Kumar et al. (2021) studied the materials used to construct such buildings with meagre average consumption and the availability of renewable energy sources (mainly solar energy) to meet energy demand. Their research mainly concerns energy calculations and insulating materials in energy-efficient buildings, representing a typical passive design strategy. In addition, some researchers are interested in high-rise buildings, like Giouri et al. (2020). Their study aimed to create an integrated decision-making strategy in designing zero-energy buildings using multi-objective optimisation of building design and construction parameters for minimising energy demand while maximising energy production and adaptive thermal comfort. They proposed an integrated approach to a typical high-rise office building in Greece. Moreover, a review of the assessment of renewable energy generation for net-zero energy buildings is presented by Ahmed et al. (2022). They discussed the contribution of renewable energy generation (hydropower, wind, solar, heat pumps, and bioenergy) to developing net-zero energy buildings and reviewed their role in addressing the decarbonisation challenge. However, a different definition of net-zero energy building may also lead to new strategies. A comprehensive case study is presented by Ahmadi et al. who demonstrate how the proposed new definitions of a net-zero energy building can be applied to promote their net-zero energy building system (Ahmadi et al., 2021). Hamza et al. integrated photovoltaic technology to explore the potential for achieving nZEB levels in Egypt through retrofitting buildings (Hamza et al., 2022). She et al. studied the multi-objective optimisation of zero-energy buildings, including the efficiency of solar energy use (She et al., 2021).

In most studies on zero-energy buildings, photovoltaic and wind are the most commonly used renewable energy sources. However, in a city like Hong Kong, where minimal land is available, it is challenging to use renewable energy to bring high-rise buildings up to zero standards. The development of ocean energy should also be explored more, considering the advantages of coastal geography. From 2019 to 2020, marine technology was

estimated to increase power generation by 400 GWh, a percentage increase of 33% (IEA, 2021c). In the IEA Ocean power report, while advanced marine power projects in the range of 10 kW to 1 MW have been deployed, these demonstration and small commercial projects are still expensive because the economies of scale needed to reduce costs significantly have not yet been realised (IEA, 2021c). The last decade has seen the emergence of many new wave energy applications in Europe, such as the Pantelleria wave energy plant in Italy, a 0.05 MW project active from 2019 (IRENA, 2020). There is also a 0.15 MW project in France called WAVEGEM® in the SEMREV test project (IRENA, 2020; SEM-REV, 2019). More marine energy in Asia is concentrated in tides, such as the LHD tidal project in China and the Sihwa-ho tidal power plant in South Korea (IEA, 2021c; iha, 2016; Li et al., 2022; SEM-REV, 2019). Moreover, there are also some studies on the energy of ocean currents, concentrated more on Japan and Taiwan, China (Corportation, 2014; Hsu et al., 2015). In addition to the applications or demonstrations, and research of marine renewable energy systems, there have been some studies on the interaction between buildings and renewable energy sources. For example, Zhou et al. (2022) applied the hybrid ocean thermal, floating photovoltaic and tidal stream generators to support a coastal zero-emission office building. The technical and economic feasibility of hybrid ocean energy for hotel buildings has been studied by Luo et al. (2022) and Guo et al. (2021). Luo et al. investigated a hybrid system with offshore wind turbines and wave energy converters, and Guo et al. studied a hybrid system with floating photovoltaic and wave energy converters. Meanwhile, Li et al. (2022a) conducted a techno-economic analysis of large-scale hybrid ocean energy that supports communities.

1.2.2. Electric mobility with renewables

Electric vehicles (EVs) are the mainstream means of transport to be promoted in the following decades. More and more studies presented the interaction of electric vehicles with the grid and buildings. Yan et al. (2020) investigated the optimal planning of distributed wind and solar capacity to improve renewable electricity supply to charge electric vehicles based on simulated area profiles. The paper of Li et al. (2022b) considers a microgrid consisting of distributed power sources such as wind and photovoltaic, electric vehicle charging stations, and energy storage systems. The charging demand of electric vehicles and the uncertainty of distributed renewable energy output were incorporated. Based on the road network and grid combination, a robust optimisation model for the location of distributed energy charging stations was proposed. Zandrazavi et al. (2022) presented a study on stochastic multi-objective optimal energy management for grid-tied unbalanced microgrids with renewable energy generation and plug-in electric vehicles. Xu et al. (2021) proposed a new, cost-effective, commercial building-oriented power supply system with PV support for shopping centres. They also considered electric vehicles and modelled them separately according to different stochastic behaviours. As a result, they found that applying PV and retired electric vehicle batteries is beneficial for commercial buildings. Cao (2019) investigated the impact of EVs and mobile boundary expansions on a zero-emission building; the building is supported by solar and wind energy. Feng et al. proposed an optimal dispatch strategy for power system flexibility considering renewable energy and electric vehicles (Feng et al., 2022).

In addition to EVs, the interaction between metro systems and the grid has received some attention. For example, Kumar and Cao (2021) conducted six different metro-rail systems comprehensively developed and comparatively studied to investigate the integration of renewable energy sources and the interaction between metro stations. The integration of renewable energy sources and the interactions among metro stations, metro trains, and the utility grid were studied alongside optimal load matching and grid interaction. Al-Janahi et al. (2020) also studied the techno-economic feasibility of the grid-connected building-integrated photovoltaic system with the metro in Duha.

On the other hand, there have been some studies on electric boats. Tercan et al. (2021) presented three sustainable transport designs and designs for grid-connected power stations using photovoltaic panels. They analysed their feasibility as alternatives to diesel-powered tourist boats. These studies suggested that various off-grid rooftop photovoltaic systems could be suitable for sustainable transport while reducing the operating costs of boats. Wang et al. (2021) brought a study on fast catamaran ferries with battery power and a comparative assessment with the respective conventional ferries, revealing the advantages and disadvantages of these two alternative solutions. The reference Huang et al. (2021) investigated the current development and application of solar energy, wind energy, and fuel cell in ship power systems. The application of renewable energy technologies, such as solar, wind, and fuel cells, to optimise the energy mix of ships is beneficial both economically and environmentally.

Previous work (Guo et al., 2021) on "The Feasibility of Using Zero-Emission Electric Boats to Enhance the Techno-Economic Performance of an Ocean-Energy-Supported Coastal Hotel Building" discussed how different combinations of FPV and WEC can lead to a better energy matching capability, these non-dominated results of building-to-boat and boat-to-building functions on the system at different cruising speeds and distances were also observed. The results presented that when the total annual generation ratio of WEC and FPV are 66% and 34%, this combination could achieve the best energy-weighted-matching index. Therefore, these non-dominated results (the best results among the cases that have been studied) from the previous work are applied directly in the current study. The previous article has demonstrated the economic feasibility of the hybrid system. However, the study did not investigate the technical and economic impact of the boat energy system. For example, previous work has not focused on the application of boat batteries for energy storage and energy flexibility control. Moreover, the tariff model used in the previous study was a single-model and did not consider peak and off-peak electricity consumption and demand charges.

1.2.3. Energy flexibility with valley-filling and peak-shaving

Energy storage, energy matching, and energy flexibility are increasingly investigated and analysed in most energy interaction studies. Many studies have also focused on applying electric mobility (e.g., EVs) to enhance a better energy management system. For instance, Yu Wang et al. (2019) proposed a multi-agent system to investigate the peak-shaving potential of EMS in high-rise residential buildings equipped with PV storage systems. Zhan et al. devised a decentralised control method to schedule EV charging loads to fill the load valleys at night while meeting the charging requirements of customers (Zhan et al., 2015). Ioakimidis et al. (2018) also researched peak shaving and valley-filling of power consumption profiles in non-residential buildings using an EV parking lot. They used MATLAB to model the power consumption curve of a university building by scheduling the charging or discharging process of an EV car park, using real-world power consumption and car park occupancy data to shave off the peaks and valleys. The study Campana et al. (2021) introduced lithium-ion batteries as an energy storage unit in the commercial sector by considering a representative building with PV systems. The battery strategy helps eliminate target peaks, perform price arbitrage, and increase PV self-consumption. The reference Al-Bahrani et al. (2020) studied EVs' dynamic economic emission scheduling and load demand management during peak and valley reduction in a smart city. Zhang et al. (2014) presented

a novel decentralised valley-filling strategy that optimises vehicle charging in a grid–EV system. Moreover, Ma et al. (2022) focused on valley-filling pricing for charging EVs considering renewable energy generation. Their paper aims to guide the coordinated charging of EVs and help achieve valley-filling by designing a time-of-use pricing mechanism. Ma et al. investigated a demand response-based business model and operational strategies for user-side storage devices, in which a business model based on a peak-to-valley arbitrage strategy was proposed (Ma et al., 2021).

1.3. Scientific gaps

Based on the above literature review, several scientific gaps in the international academic community can be noted:

First, the existing interaction between buildings and renewable energy primarily relies on onshore solar and wind energy, while limited studies have focused on marine energy, as current small-scale commercial projects are not significantly cost-effective. Nevertheless, studies and surveys (e.g., Guo et al., 2021; Luo et al., 2022; Zhou et al., 2022) have shown that economic benefits from small-scale hybrid ocean renewable energy can be potentially significant. Rare studies are proposed to investigate how these benefits can be further enhanced by improved energy flexibility controls.

Second, while many articles have discussed the interaction between EVs and renewable energy, there have been few research results on ocean energy. The energy interaction with electric metro rail systems has also been studied in some papers (Kumar and Cao, 2021; Al-Janahi et al., 2020). However, the interaction among electric boats, the grid, and renewable energy, especially ocean energy, is limited. In a city like Hong Kong, where land space is limited and expensive, the development of ocean renewable energy is more promising and feasible than traditional land-based renewable energy.

Third, the existing studies on energy flexibility of valley-filling and peak-shaving have proven effective in grid stability and economy. EV as an intermediary for energy storage has also proven feasible. However, there is still a lack of comprehensive studies investigating the techno-economic and environmental feasibility of electric mobility in ocean renewable energy systems for valley-filling and peak-shaving.

In summary, the central novelty aspect and the contributions of this study are:

(1) Flexibility and feasibility of hybrid ocean energy sources: This article discusses and investigates the interaction between marine renewable energy and small-scale commercial building to demonstrate the feasibility of hybrid marine energy, and it focuses on the technical and economic performance of the whole hybrid system, taking full advantage of the flexibility control strategy, which is less available with conventional controls.

(2) Ocean Energy flexibility control via electric boats: In previous studies, EVs have been discussed more often, and electric boats have rarely been mentioned. However, electric boats are more beneficial than EVs in harnessing marine renewable energy and have more specific cruising characteristics and demand requests than EVs. This study shows how electric boats can be used as a mobile energy storage system and can also be used to achieve energy flexibility control, which has rarely been mentioned in previous studies.

(3) Multi-objective analysis and investigation of hybrid systems with flexibility control: Peak-shaving and valley-filling, as common flexibility control strategies, are usually focused only on economic performance. This paper brings a more comprehensive, multi-objective analysis and investigation is carried out in this study, which is very limited in previous studies.

(4) Five flexibility control strategies are conducted based on the previous study: Previous work focuses only on building-to-boat and boat-to-building functionality and does not involve any flexibility controls, given that the tariff model does not take into account peak and off-peak. Conventional controls would store surplus renewable energy and discharge marine batteries when building demand is a shortfall. This untargeted charging and discharging did not make full use of the potential of the battery as a source of flexibility. This paper brings a non-dominated solution to this gap with five flexibility control strategies.

Based on these three scientific gaps, this paper proposes an innovative and integrated energy flexibility control strategy for grid valley-filling and peak-shaving. The aim is to shift electricity peaks to off-peak periods of a hotel building as much as possible by using batteries from electric boats as movable energy storage sources, supported by a hybrid renewable energy source. Furthermore, a comprehensive techno-economic-environmental investigation and analysis of the simulation results are presented. In the reminder of this paper, Section 2 introduces the information about the hybrid system and the assumption. Section 3 presents the flexibility control logic of the E-boats for both basis control and improved control; a detailed schematic diagram is introduced to explain the control process. Key indicators and analysis criteria of energy matching and flexibility capabilities are proposed in Section 4. Section 5 shows the control result for two reference cases and five flexibility control strategies. Each control strategy inherits the non-dominated result from the previous one; therefore, strategic E presents the final control result. The conclusion is summarised in Section 6.

2. System modelling description and assumptions

As presented in Fig. 1, ocean energy supports the hybrid zero-energy building, and the seawater-transportation system relies on three main components: the building system, the hybrid renewable generation system, and the electric boat system. The hybrid renewable energy generation systems consist of floating photovoltaic panels (FPV) and wave energy converters (WEC). The simple energy management solution is to use renewable energy generation to support the needs of the hotel. When there is surplus generation, after the building demand has been satisfied, the rest of the surplus energy is sent to the battery to be charged and fed into the grid. Conversely, when there is an energy shortage in the building, the boat battery discharges itself and feeds the remaining energy shortage from the grid. The detailed energy flexibility controls are presented in Section 3.

The modelling and basic information about these systems are presented in the following sub-sections. All the components mentioned are modelled and performed in TRNSYS 18. TRNSYS is a transient system simulation program, commercially available since 1975, with a flexible software environment for simulating the behaviour of transient systems. It is mainly used for energy system design and building simulations (Madison, 2022). The software has individual component models, called “TYPE”, which can be interlinked to simulate a near-realistic environment to study various energy and building systems, such as HVAC systems, energy storage systems, and renewable generation systems. In this study, the simulation time step is 0.25 h, ensuring the stability and convergence of the system models. Table 1 reports the key information and parameters assumed in this study, and detailed information on these parameters and assumptions are introduced in the following sub-sections.

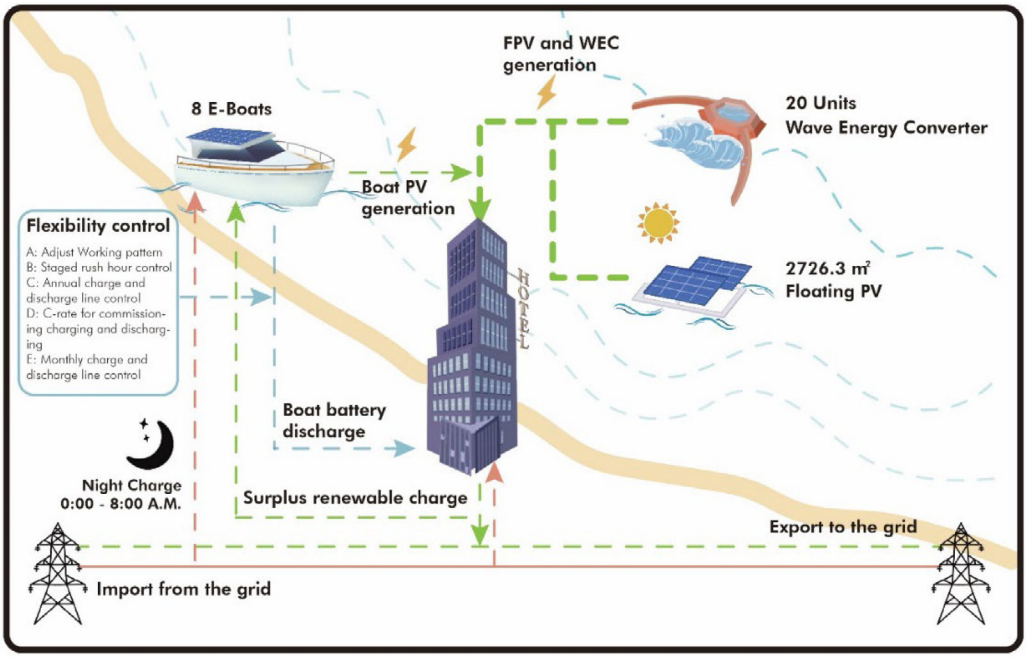

Fig. 1. The schematic of the ocean energy supported the hybrid zero-energy building and seawater-transportation system.

Table 1
Key information and parameters are assumed in this study.

Items	Key information/parameters of assumptions	Reference
Hotel Building	Located on Cheung Chau Island, Hong Kong SAR, 8 floors, 480 m^2 on each floor, a total area of 3840 m2	The Performance Based Building Code of Hong Kong (EMSD, 2007)
Floating PV	2726.3 m^2 FPV are equipped, and the rated capacity of each module is 260 W.	(FuturaSun, 2022)
Wave energy converter	20 units of WEC are applied, and each WEC has a 20kW rated capacity.	(Parmeggiani et al., 2011; Wave Dragon, 2022; Wave dragon 1.5 MW, 2015))
Zero-emission electric boat	Eight boats serve the hotel, each with two marina-grade lithium polymer batteries with a total capacity of 120 kWh.	(SOELCAT 12, 2022)

2.1. Weather and building service system

The studied coastal hotel building is assumed to be located in Hong Kong Special Administrative Region, Cheung Chau Island. Hong Kong's climate is subtropical, tending toward temperate for nearly half the year (Observatory, 2020). The weather data source for this study is one year's data compiled from 20 years of records in the Meteonorm database (Meteonorm, 2022; Solar Energy Laboratory of the University of Wisconsin-Madison, 2017). Based on the database, the monthly solar radiation, dry bulb and wet bulb temperatures can easily be analysed and investigated. As can be seen from Fig. 2, the total monthly solar radiation varies from 64 kWh/m^2.mon(February) to 168 kWh/m^2.mon(July). Dry bulb temperatures vary throughout the year, almost similar to solar radiation, with a maximum average high of 28.8 °C in July and a minimum temperature of 15.8 °C in February. Wet-bulb temperatures are around 2.4 °C to 3.9 °C lower than the average dry bulb temperature in each month.

The seawater temperature data is from the Hong Kong Observatory, and it is historical data for 2017 recorded from Waglan Island. The average seawater temperature in Hong Kong throughout the year is 22.5 °C, with January and February being 1.3 and 1.1 °C above the dry-bulb temperature, March and September to December being about the same as the monthly average dry-bulb temperature, and April to August being cooler, about 0.7 to 2.6 °C below the dry-bulb temperature.

Fig. 3 illustrates the monthly significant height of the wave in Hong Kong, recorded from the West Lamma Channel monitoring station. The data source is the significant wave heights at hourly intervals provided by the Hong Kong Civil Engineering and Development Department. In this study, the year of data used for the specific simulation is 2019. However, the historical records in 2019 had missing data at some time; data from 2017 and 2018 supplemented the missing data. In Fig. 3, the monthly average significant wave heights in Hong Kong range from approximately 0.25–0.47 m. February is the worst, with daily average minimum wave heights in the vicinity of 0 m.

The coastal hotel building understudy is assumed to be on Cheung Chau Island, close to Lamma Island. The hotel building was designed and modelled as a new building, with the design criteria following the Performance Based Building Code of Hong Kong (EMSD, 2007). The hotel building has eight floors above ground, 480 m^2 on each floor with a height of 3 m and a total area of 3840 m^2. Detailed design and modelling parameters for the building envelope, insulation, and electrical service system are listed. Appendix A includes 7 essential parts: insulation, infiltration, occupants, ventilation, AHU cooling and heating, space cooling and DHW. These design parameters and principles of the hotel building envelopes, insulation and services systems determined the cooling and heating demand of the hotel building.

(1) The insulation has four parts: the external roof, wall, window glazing, and ground floor layer with soil layer, the

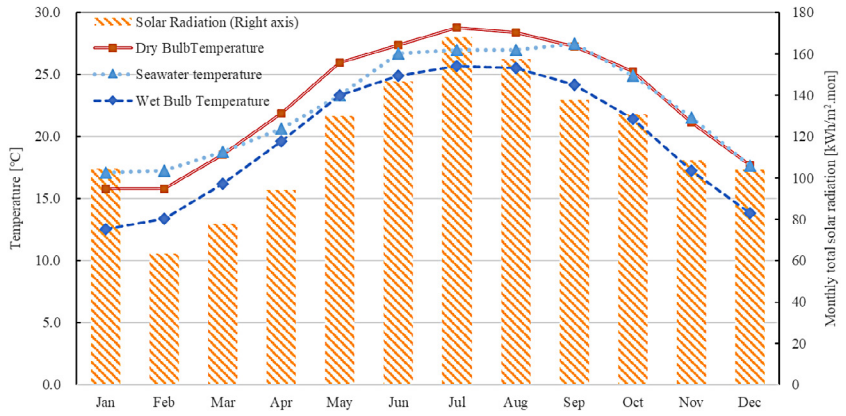

Fig. 2. The monthly dry and wet bulb temperature, seawater temperature, and the total solar radiation in Hong Kong.

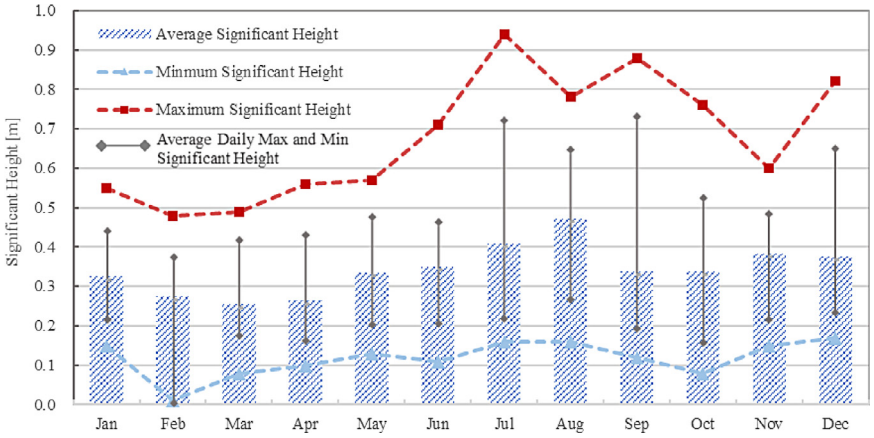

Fig. 3. The monthly significant height of the wave in Hong Kong, West Lamma Channel.

U-value of these components are 0.345, 2.308, 2.78 and 0.609, respectively.

(2) As for the infiltration, when the ventilation is on, the value is 0.306 h-1; when the ventilation is off, the value is 0 h-1.
(3) The designed occupants for each floor are 19 people, which is based on the guideline of the Performance-based (EMSD, 2007); the activity level MET is 1.2 in this building.
(4) The ventilation system is mechanical supply and exhaust ventilation with return air mixing and rotary heat recovery. The supply flow rate is 1.5 h-1 when the fan is on. The fresh air ratio in the total supply air flow rate is 0.475.
(5) The AHU cooling method in this building is a 7/12 °C cooling coil, and the AHU and Reheate heating method is hydronic heating. The in-blown supply air temperature follows a function concerning the exhausted indoor air temperature. The sensible and latent effectiveness of the rotary heat recovery device is 0.85 and 0.5, respectively. The specific ventilation fan power of the supply and exhaust fan is the same as 800 W/(m^3/s).
(6) The space cooling applies a hydronic chilled ceiling system; the set point is 15/17 °C, and the room air set point is 24 °C for all thermal zones. As for the space heating, electric heating is equipped; the room air set point is 21 °C for all thermal zones.
(7) The DHW heating is set at 55°C, and the daily consumption volume is 17.8 m^3.

Table 2 reports the total annual energy demand and peak power demand for air handling unit (AHU) cooling, space cooling, AHU heating, space heating, domestic hot water heating, reheater heating and building electrical demand. Fig. 4 represents the duration curve of cooling, heating, and electric demands of the hotel building. Cooling is the largest energy consumer on this list, three times more than heating. The annual energy demands for cooling, heating and electricity are 205.99, 67.85, and 102.7 kWh/m^2.a, respectively. The peak power is 227.82, 75.7, and 100.94 kW, respectively. According to the information in Table 2, AHU cooling has the highest energy and electricity demand of all. The second largest consumer is electric, including lighting, equipment and ventilation fans, but not cooling and heating systems or electric boats.

2.2. Hybrid renewable system

Based on the former study (Guo et al., 2021), the hybrid renewable Wave-FPV system shows its highest energy Weighted Matching Index (WMI) result when the total annual generation of wave energy converter (WEC) and FPV is 74% and 26%. However, this mixing ratio is difficult to have a positive relative net present value (NPV_{rel}) within 20 years of lifetime. Therefore, as shown in Fig. 1, the Wave-FPV mixing generation ratio in this study adopted 49% and 51%, which means 2726.3 m^2 of FPV and 20 units of WEC are equipped to support the building.

2.2.1. Floating photovoltaic panel (FPV)

Floating photovoltaic panels are assumed to be installed in the sea near the hotel. The simulation model in TRNSYS for the FPV is Type 567. Type 567 is a model used for modelling building the integrated photovoltaic system. The idea is to set up the seawater temperature instead of the ground temperature via setting the

Table 2
The cooling, heating, and electric demands of the studied coastal hotel building.

	Cooling			Heating				Reheater	Electric[b]
	AHU Cooling	Space Cooling	Total Cooling	AHU Heating[a]	Space Heating	DHW Heating	Total Heating (Excluding Reheater Heating)	Reheater Heating	Electric[b]
Total Energy (kWh/m^2.a)	164.88	41.10	205.99	0.01	0.06	67.78	67.85	15.60	102.70
Peak Power (kW)	146.78	98.49	227.82	22.50	7.59	68.40	75.70	14.79	100.94

[a]AHU heating demand does not include the demand for reheaters equipped with cooling coils.
[b]Electric demand includes lighting, equipment and ventilation fans but does not include cooling and heating systems or electric boats.

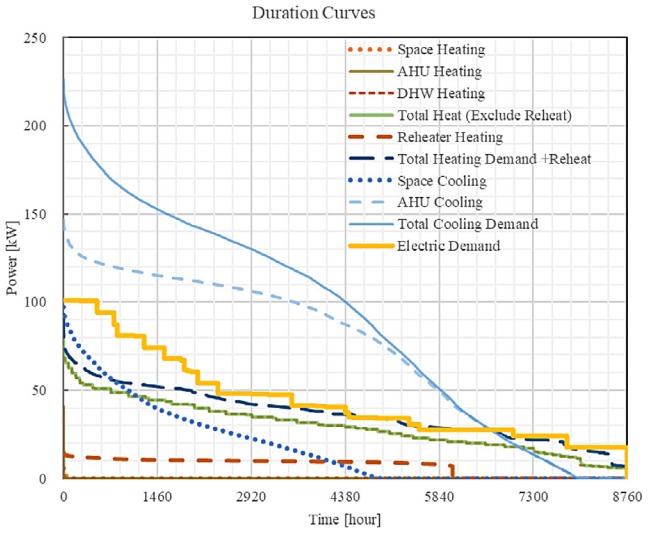

Fig. 4. The duration curve of the cooling, heating, and electric demands of the hotel building.

back-surface temperature in Type 567. As mentioned in the previous sub-section, the one-year seawater temperature data used for simulations were from the Hong Kong Observatory and were recorded from Waglan Island in 2017. The parameter modelling FPV in TRNSYS is a commercial product called FuturaSUN (FuturaSun). The product is a polycrystalline silicon PV product with 60 cells per module. The dimension of the equipped FPV (FU 260P) is 1650*990*35 mm, and the efficiency of the product is published as 15.92% under standard test conditions. The rated capacity of each module is 260 W.

2.2.2. Wave energy converter (WEC)

The 20 units of wave energy converter are also assumed to be applied in the sea around the hotel. The model information of the wave energy converter in TRNSYS is also based on a commercial product called "Wave dragon". This generation system has crab-shaped arms that collect the instantaneous wave to its reservoir. The reservoir uses the potential energy of gravity to drive the turbines at the bottom of the system to generate electricity when the seawater is released. The primary data driving this power generation system is the significant height of the local waves. The historical data used in this study is from the West Lamma Channel monitoring station. Each WEC has a 20 kW rated capacity. The previous study studied the equations for hydroelectric power generation, referring to the literature (Parmeggiani et al., 2011; Wave Dragon, 2022; Wave dragon 1.5 MW, 2015). Readers interested in the generation system are recommended to read the papers cited.

2.3. Zero-emission electric boat

In this study, eight electric boats serve the hotel complex for tourism. The model information for this zero-emission electric boat comes from a Netherlandish commercial product, the "Soelcat 12" (*SOELCAT 12*), with a capacity of 12–20 people per boat. Eight boats are a reasonable design volume for the hotel, considering the maximum occupancy is designed as 19 people per floor. During the TRNSYS modelling process, the boat was simulated with two main components: its own battery and its own roof photovoltaic panels. Each E-boat is equipped with two marina-grade lithium polymer batteries with a total capacity of 120 kWh. Replacement is considered when the batteries have exceeded 2000 cycles. The battery model used TYPE 47a in TRNSYS. For the boat PV, due to the insufficient information from the boat manufacturer, the boat PV model information came from another commercial product: LG NEON (LG, 2022), a monocrystalline silicon product with high efficiency of around 19.7%. Each E-boat has 25 units of PV with a total capacity of 8.5 kWp. The detailed control principle and cruising mode of E-boats are introduced in Section 3.

Based on the previous study for the various cruising velocity and distances (Guo et al., 2021), the weighted matching index (WMI) would be its maximum when sailing at 15 km/h for 7.5 km. In this study, the cruising velocity and distance are assumed as constant at 15 km/h and 7.5 km. Therefore, the constant energy consumption of the E-boat is fixed at around 1.13 kWh/km. Readers interested in the energy requirements of boats affected by various speeds and distances are recommended to read the previous research paper.

It is worth mentioning that the battery model is based on the cycle life of the battery in this study, which according to the manufacturer of E-boats, is 2000 cycles. As in this study, the sailing distance and frequency were not very long and high, the FSOC for charging and discharging was between 0.95 and 0.25, and there was no over-charge or over-discharge. Therefore, this study does not consider long-term life degradation, and the E-boats replace the batteries after they have reached 2000 cycles and consider the residual value of the batteries if they have a remaining number of cycles in their 20-year life cycle. The specific economic modelling formulae for the life cycle and salvage value will be shown in Section 4.

3. Building services and integrated boat energy systems with their flexibility sources

3.1. The basic components, final control principles, and associated flexibility sources

The control strategy of the hybrid system is depicted in Fig. 5. The holistic control strategy could be broken into three parts: generation, boat-to-building, and building-to-boat. When two fleets of boats are at the pier, their roof photovoltaic panels

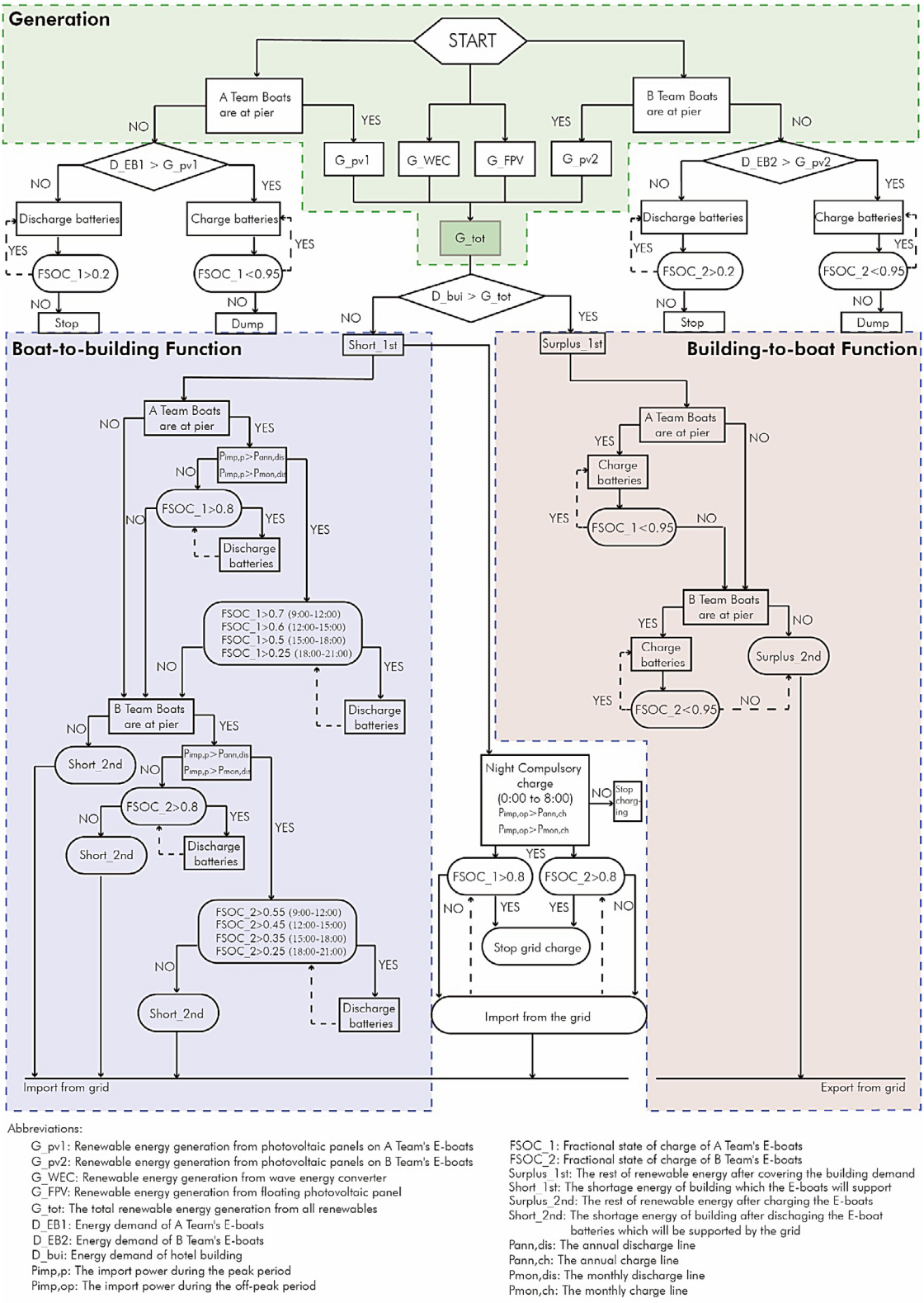

Abbreviations:

G_pv1: Renewable energy generation from photovoltaic panels on A Team's E-boats
G_pv2: Renewable energy generation from photovoltaic panels on B Team's E-boats
G_WEC: Renewable energy generation from wave energy converter
G_FPV: Renewable energy generation from floating photovoltaic panel
G_tot: The total renewable energy generation from all renewables
D_EB1: Energy demand of A Team's E-boats
D_EB2: Energy demand of B Team's E-boats
D_bui: Energy demand of hotel building
Pimp,p: The import power during the peak period
Pimp,op: The import power during the off-peak period
FSOC_1: Fractional state of charge of A Team's E-boats
FSOC_2: Fractional state of charge of B Team's E-boats
Surplus_1st: The rest of renewable energy after covering the building demand
Short_1st: The shortage energy of building which the E-boats will support
Surplus_2nd: The rest of renewable energy after charging the E-boats
Short_2nd: The shortage energy of building after dischaging the E-boat batteries which will be supported by the grid
Pann,dis: The annual discharge line
Pann,ch: The annual charge line
Pmon,dis: The monthly discharge line
Pmon,ch: The monthly charge line

Fig. 5. The final flexibility control of the hybrid system.

also provide renewable energy to the building side. Therefore, the total generation is the sum of boat PV (G_pv1, G_pv2), FPV (G_FPV), and WEC(G_WEC). The boat-to-building function will be activated when the building demand exceeds the total generation, also called "Short_1st". However, the activation conditions for the A team of E-boats and the B team are different. The specific activation conditions are described in Section 3.2.2 and shown in Fig. 5. If the building is supported by the boat-to-building function in A Team and B Team, when there is still a building energy deficit, the remaining energy is brought in directly from the grid, which is named "Short_2nd". When the total generation is larger than the building demand, the surplus energy is called

Table 3
The basic control principle of the reference system.

Working mode and schedule	No. of E-Boat teams and E-boats:	1 team and 8 boats (all boats cruise out together)
	Tour schedule:	9:00-22:00, 2 h per tour, each tour 30 min, every day has 7 tours
	Cruise mode:	7.5 km, 15 km/h
Charging mode (Building-to-boat function)	Renewable surplus charging:	24/7h (Charging range of FSOC: 0.95 to 0.3)
	Grid charging:	0:00-8:00 (Charging range of FSOC: 0.85 to 0.3)
	Charging rate:	0.2C
Discharging mode (Building-to-boat function)	Discharging conditions:	Off-work, Energy Deficit of building, not in charging mode, 24/7h (Discharging range of FSOC: 0.95 to 0.8)
	Discharging rate:	0.2C

"Surplus_1st" the building-to-boat function would be activated if the boats are at the pier. The boats would be charged to the highest possible limit FSOC (0.95) of their batteries. After charging, if there is still any surplus renewable, the rest energy would be sent to the grid, called "Surplus_2nd".

Flexibility is a capability that can react to the performance and requirements of a system. The energy flexibility of a building is reflected by the readiness and energy response of the buildings involved in the building energy system (Zhou and Cao, 2020). In this study, flexibility is the ability to cut peaks and fill valleys. The main objective of the proposed flexibility control is to improve the technical performance of this hybrid system while simultaneously improving economic performance and paying attention to environmental performance. This flexibility control targets a multi-objective control; the detailed indicators of these performances are introduced in Section 4.

In this study, as shown in Fig. 5, rule-based control was performed rather than optimisation-based control. In general, optimisation-based control focuses on a greater number of variables which are more complex and comprehensive. In this paper, we focus more on those key variables that are more sensitive and responsive to flexibility control, which is the main reason for conducting a parametric analysis rather than an optimisation-based analysis. On the other hand, the primary source of energy flexibility in this paper is boat batteries, with five targeted strategies such as commissioning different FSOC, and annual and monthly controls to rationalise discharge during certain peak hours or charging during low hours. This rule-based control also brings weakness, considering other variables were not under investigation; therefore, other variables may be able to optimise the performance of the system further. However, these results did not appear in the previous non-dominated results. However, this study discusses the most sensible variables as comprehensively as possible. More comprehensive optimisation-based control and analysis should be the future work to complement and update the conclusions and results of this paper.

3.2. The control principles and associated flexibilities for integrating the zero-emission electric boat

3.2.1. The basic control principle of the reference E-boat system

The reference system of this study concerns the hotel building with eight zero-emission electric boats. The basic control principle is followed in the previous study, which has a non-dominated on-site renewable energy matching capability and beneficial NPV_{rel}. The basic control principle is shown in Table 3.

First, 8 E-boats are working for the hotel building; these E-boats cruise around the sea area together from 9:00 to 22:00 every day. The daily boat tours are be at 2-h intervals, each tour would last half an hour, and the cruising distance is 7.5 km, assuming the cruising speed is maintained at 15 km/h. Based on the previous study (Guo et al., 2021), the energy consumption with this cruising plan is around 1.13 kWh/km. Second, the activation of the building-to-boat function has two modes and one condition. The charging mode can be activated when there is a surplus of renewable energy; this mode can occur at any time of the day as long as the boat battery is not saturated with FSOC (Saturated FSOC is 0.95).

Meanwhile, the batteries can be charged from the grid from 0:00 AM to 8:00 AM to ensure the boat sails appropriately during the day, provided that the FSOC is below 0.85. All are charging C-rate is default to 0.2C, which means a full battery charge takes five hours. In the reference system, the E-boat also provides a boat-to-building function. In other words, the boat can discharge its own batteries to provide parts of the energy for the building. This function can only be activated if the E-boat is moored in port, there is an energy deficit in the building, the E-boat is not being charged from the grid, and the boat battery has an FSOC above 0.8. Similarly, the C-rate of the discharge mode defaults to 0.2C.

Table 3 reports the basic controls from the previous study, with default upper and lower charging FSOC limits of 0.95 and 0.3, respectively. This default FSOC setting can help avoid over-charging and over-discharging. Therefore, when renewable energy sources charge the electric boat, the FSOC ranges from 0.95 to 0.3, which means charging to full as much as possible. However, when renewable energy is insufficient and the electric boat needs to be charged from the grid, the upper limit of FSOC is reduced to 0.85. This setting not only ensures the need for at least one day of touring activities but also leaves a buffer to charge the battery through renewable energy. As for the discharged FSOC, the lower limit is 0.8, which is the minimum discharge value to protect the battery with enough energy for the rest of the daily cruising.

3.2.2. Flexibility control principle of E-boats

Table 4 shows the new control principle of E-boats, the operating mode of boats changes to two teams. Each team has 4 E-boats, and these 4 boats cruise out together. Two boat teams have a cross-working schedule, as illustrated in Fig. 6. The A team (red dot and line) has a tour activity from 9:00 to 21:30, working at 2-h intervals; each tour lasts half an hour. The B team (yellow dot and line) keeps the same working pattern, while the working time is 10:00 to 22:30. The cross-working plan for the two fleets considers the idea that there hopefully always be boats interacting with the buildings. This new working schedule helps improve the energy flexibility of the holistic system. It is worth noting that this new cross-working plan, which also ensures the

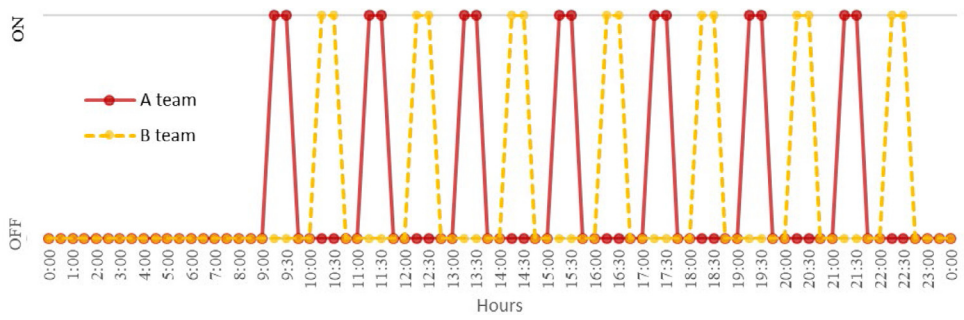

Fig. 6. The working schedule for two E-boat fleets.

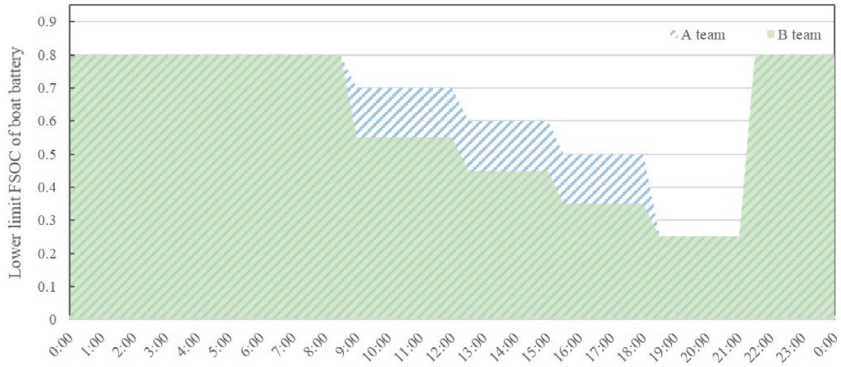

Fig. 7. The daily peak period control and phased deep discharge schedule for lower limits of boat batteries.

Table 4
The flexibility control principle of the reference system (the underline shows the change after improved control).

Working mode and schedule	No. of E-Boat teams and E-boats:	2 teams and each team has 4 boats (two teams have crossed schedule, as detailed in Fig. 6)
	Tour schedule:	9:00-22:00, Crossed Schedule
	Cruise mode:	7.5 km, 15 km/h
Charging mode (Building-to-boat function)	Renewable surplus charging:	24/7h (Charging range of FSOC: 0.95 to 0.2)
	Grid charging:	0:00-8:00 (Charging range of FSOC: 0.85 to 0.2)
	Charging rate:	0.2C to 2C (investigated in section 5.2.4)
Discharging mode (Building-to-boat function)	Discharging conditions:	Off-work, Energy Deficit of building, not in charging mode, peak period control with staged deep discharge plan (as detailed in Fig. 7)
	Discharging rate:	0.2C to 2C (investigated in section 5.2.4)

same total annual energy consumption for all boats, allows the new controls to be compared with the reference case.

In the improved control, the boat batteries could be deeper discharged to 0.2 (FSOC). Therefore, the new charging range is 0.95 to 0.2 and 0.85 to 0.2 for renewable and grid charging, respectively. The charging rate is a variable and is investigated in the following section. As for the discharge control, the discharging period only occurs in the peak period, and the discharging FSOC has a particular discharge schedule considering both fleets' working schedules. Fig. 7 presents the daily discharge schedule for lower limits of boat batteries. For A Team, during the off-peak period, batteries could still be discharged to 0.8 (FSOC); the peak period is divided into 4 phases 9:00 to 12:00, 12:00 to 15:00, 15:00 to 18:00, and 18:00 to 21:00, these periods correspond to their lower limit discharge FSOC of 0.7, 0.6, 0.5 and 0.25 respectively. The main discharge period for A-Team is the evening rush hour from 18:00 to 21:00; this phased arrangement ensures the normal tour functions while avoiding excessive discharge before the evening peak.

Similarly, the lower discharge limits of FSOC for the B Team are 0.55, 0.45, 0.35, and 0.25 for the corresponding periods. The main discharge period for B Team is the morning rush hour from 9:00 to 12:00. Two E-boat fleets have a special discharge schedule that may help shave the peak power, especially during the morning and evening. The discharge rate varies from 0.2C to 2C, and the corresponding enhancement of flexibility is investigated in Section 5.

There are three main reasons to conduct the flexibility control with the E-boats in the current: First, although E-boats are not as widespread as EVs, it is clear that E-boats have more access to ocean energy than electric vehicles, considering E-boats have more regular and fixed interaction conditions and patterns.

Secondly, E-boats are more susceptible to disturbances in the demand pattern than EVs, significantly as cruise distance and speed affect the consumption of the boat batteries. However, in urban areas, changes in the speed of EVs do not cause significant changes in energy consumption, so E-boats have more sensitive variables affecting energy consumption than EVs. This is one of the reasons why it is worthwhile to investigate the interaction separately. Finally, most traditional interactions between mobile transport and buildings have only discussed simple V2B or B2V functions. There is a very limited study that investigated how to make full use of the batteries of these EVs for energy flexibility control to improve the overall performance of systems with erratic power generation characteristics, such as ocean energy. This is one of the objectives of this paper.

4. Analysis criteria

Several critical indicators are introduced to investigate and compare the techno-economic performance of the system. The new indicators focus on peak-shaving and valley-filling capacity in terms of flexibility. The environmental performance is addressed with an emissions indicator. As the leading indicators to investigate the renewable energy matching capacity, the index of on-site energy fraction (OEF) and the on-site energy matching index (OEM) are applied in this study; these indicators are introduced in the study of Cao et al. (2013). OEFe represents the proportion of the on-site electrical demand covered by the on-site generation, whereas OEMe indicates the proportion consumed by the building and the system rather than being exported or dumped. The unfolded equations are shown below:

$$\mathrm{OEFe} = 1 - \frac{\int_{t_1}^{t_2} P_{imp}(t)dt}{\int_{t_1}^{t_2} [L_{elet}(t) + \frac{L_{EB_{sys}}(t)}{\eta_{EB}}]dt}, 0 \le \mathrm{OEFe} \le 1 \quad (1)$$

$$\mathrm{OEMe} = 1 - \frac{\int_{t_1}^{t_2} P_{exp}(t)dt + \int_{t_1}^{t_2} P_{dump}(t)dt}{\int_{t_1}^{t_2} P_{OREe}(t)dt + \int_{t_1}^{t_2} P_{EB_{pv}}(t)dt}, 0 \le \mathrm{OEMe} \le 1 \quad (2)$$

The $P_{imp}(t)$ is the power imported from the grid. t_1 and t_2 are the upper and lower limit of the integral standing for the starting and end of the investigated period, respectively. In this study, the simulation spans one year, therefore, t_1 and t_2 are the beginning and the end of the year. $L_{elet}(t)$ is the electricity demand power of the hotel building and $L_{EB_{sys}}(t)$ is the electricity demand power of the electric boat for excursions. η_{EB} is considered as the charging efficiency of the E-boat, which is assumed as 0.9. The P_{exp}, P_{dump} are the surplus power that is exported to the grid and dumped, the P_{OREe} and $P_{EB_{pv}}$ are the generation power from ocean renewable energy systems and the photovoltaic panels of the E-boat, respectively. It is worth noting that in this study, in order to have a better and more directive investigation and comparison, the OEFe and OEMe are analysed for the peak period of the grid and off-peak period of the grid, the equations for these four indicators are below:

$$\mathrm{OEFe,\,p} = 1 - \frac{\int_{t_1}^{t_{pp}} P_{imp}(t)dt}{\int_{t_1}^{t_{pp}} [L_{elet}(t) + \frac{L_{EB_{sys}}(t)}{\eta_{EB}}]dt}, 0 \le \mathrm{OEFe,\,p} \le 1 \quad (3)$$

$$\mathrm{OEFe,\,op} = 1 - \frac{\int_{t_1}^{t_{opp}} P_{imp}(t)dt}{\int_{t_1}^{t_{opp}} [L_{elet}(t) + \frac{L_{EB_{sys}}(t)}{\eta_{EB}}]dt}, 0 \le \mathrm{OEFe,\,op} \le 1 \quad (4)$$

$$\mathrm{OEMe,\,p} = 1 - \frac{\int_{t_1}^{t_{pp}} P_{exp}(t)dt + \int_{t_1}^{t_{pp}} P_{dump}(t)dt}{\int_{t_1}^{t_{pp}} P_{OREe}(t)dt + \int_{t_1}^{t_{pp}} P_{EB_{pv}}(t)dt}, 0 \le \mathrm{OEMe,\,p} \le 1 \quad (5)$$

$$\mathrm{OEMe,\,op} = 1 - \frac{\int_{t_1}^{t_{opp}} P_{exp}(t)dt + \int_{t_1}^{t_{opp}} P_{dump}(t)dt}{\int_{t_1}^{t_{opp}} P_{OREe}(t)dt + \int_{t_1}^{t_{opp}} P_{EB_{pv}}(t)dt}, 0 \le \mathrm{OEMe,\,op} \le 1 \quad (6)$$

The t_{pp} and t_{opp} are the annual peak and off-peak period hours of the grid, respectively. According to the reference definition of CLP (CLP, 2021a), the off-peak period of the grid is the daily period between 21:00 and 09:00 and all-day Sunday; the peak period comprises all other hours. Therefore, the annual peak and off-peak period hours are 3756 h and 5004 h in this simulation.

Based on the current policy in Hong Kong, renewable generation could receive the benefit from the feed-in-tariff; however, there is no extra subsidy for exporting renewables. The importance of OEFe and OEMe should be the same for the system. A combination indicator for OEFe and OEMe is presented to simplify the compassion of these two indicators; the weighted matching index (WMI) is shown in Eq. (7):

$$\mathrm{WMI} = w_1\mathrm{OEFe} + w_2\mathrm{OEMe} \quad (7)$$

$$\sum_{i=1}^{2} w_i = 1, 0 \le w_i \le 1, 0 \le \mathrm{WMI} \le 1$$

The WMI is calculated by multiplying the matching index by the specific weighting factor w_1 and w_2, the sum of the weighting factors should be 1.0. Higher WMI shows a higher matching capability of the system. In this study, both w_1 and w_2 are 0.5, considering the current policy shows the same significance for OEFe and OEMe. Similarly, the WMI also has WMI_p, and WMI_{op} to investigate the peak and off-peak periods separately.

Moreover, two crucial indicators are introduced to serve the flexibility capabilities. One is the Peak Shaving Indicator (PSI), and the other is the Valley Filling Indicator (VFI). PSI_p indicates the proportion of the power shaved from the reference case (benchmark) to Case j, which is the proportion of area B of area A in Fig. 8. The $P_{average,ref,p}$ is the power shaving limitation of the reference case, the annual average power imported during the peak period. The PSI_{peak} is shown in Fig. 8 and Eq. (8):

$$\mathrm{PSI_p} = \frac{\int_{t_0}^{t_{p,ref}} [P_{ref,p}(t) - P_{j,p}(t)]dt}{\int_{t_0}^{t_{p,ref}} [P_{ref,p}(t) - P_{average,ref,p}(t)]dt} = \mathrm{B/A} \quad (8)$$

The $P_{ref,p}$ and $P_{j,p}$ are the imported power of the reference case and Case j during the peak period, respectively. The $t_{p,\ ref}$ is the total target hours for shaving the peak power, which is defined by the $P_{average,ref,p}$. $P_{average,ref,p}$ is the average imported power during the peak period of one year. The t_0 is the time for the start to shave the peak power higher than the $P_{average,ref,p.}$ Moreover, $P_{average,ref,p}$ is the target line to shave all the peak power larger than $P_{average,ref,p}$ to this level. For example, in Fig. 8, the $P_{average,ref,p}$ is 100 kW, and the total hour is accumulated once $P_{ref,p}$ is larger than 100 kW, the time point of these hours is the $t_{P,\ ref}$. Therefore, when the PSI_p is equal to 1, which means the peak shaving aim is almost achieved. Meanwhile, in Fig. 8, the PSI_p stand for the area ratio of B to A. Area A represents how much peak power should be shaved in the reference case, which is the denominator in Eq. (8). Area B represents how much peak power has been shaved via the control strategies in Case $_j$, which is the numerator in Eq. (8). Once more, when the PSI_p is equal to 1, and area B equals area A, which means the power larger than the $P_{average,ref,p}$ is totally shaved. Note that PSI_p would also be larger than 1, because of the exceeded shaving beyond the $P_{average,ref,p}$.

In this study, there is another similar indicator VFI to investigate the capability of power valley-filling during the off-peak period. The VFI_{op} is shown in Fig. 9 and Eq. (9):

$$\mathrm{VFI_{op}} = \frac{\int_{t_{op,ref}}^{t_{op,end}} [P_{j,op}(t) - P_{ref,op}(t)]dt}{\int_{t_{op,ref}}^{t_{op,end}} [P_{ref,op}(t) - P_{average,ref,op}(t)]dt} = \mathrm{D/C} \quad (9)$$

The $t_{op,end}$ is the total hours of the off-peak period, which is 5004 h in this study and the $t_{op,\ ref}$ is the time for starting to fill

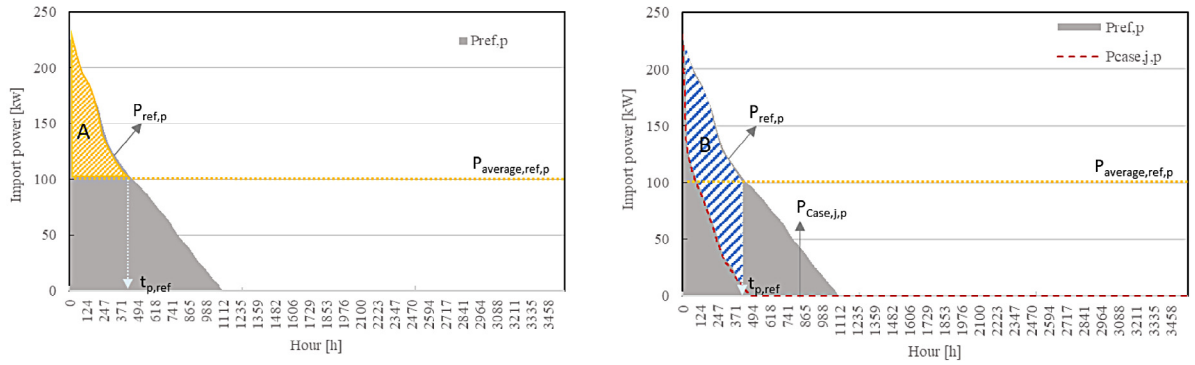

Fig. 8. The example diagram explains the Equation of PSI_{peak}. (PSI_{peak} is the peak-shaving indicator during the peak period)

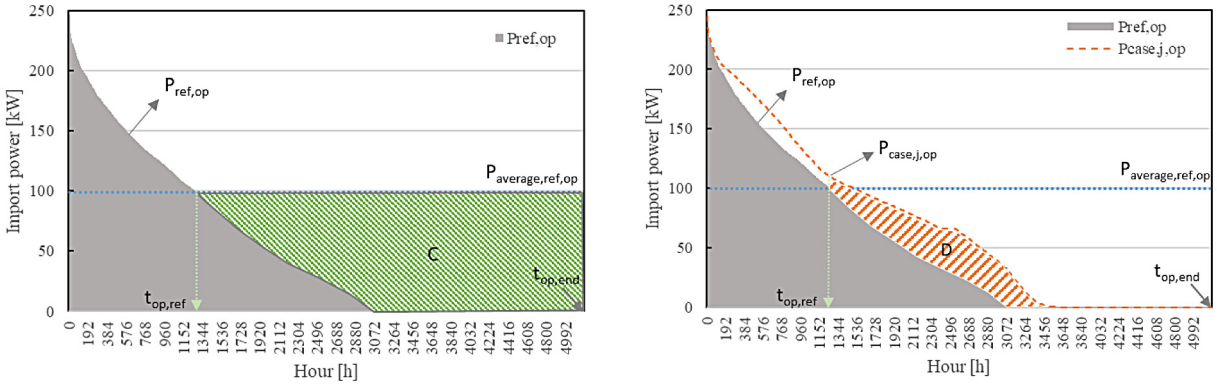

Fig. 9. The example diagram explains the Equation of VFI_{op}. (VFI_{op} is the valley-filling indicator during the off-peak period)

the peak power lower than the $P_{average,ref,op}$. The $P_{average,ref,op}$ is the average value of the imported power during the off-peak period. In Fig. 9, $P_{average,ref,op}$ is assumed as 100 kW, which means when the imported power is below 100 kW, this period is suggested to charge the battery as much as possible. In the example, Area C is the total available power that could be used to charge the E-boat batteries and static battery. Area D is the valley power filled via specific control strategies. Therefore, when VFI_{op} approaches 1 means that the power control plan of filling the valley power during the off-peak period is achieved perfectly.

Another two common indicators are introduced to investigate the economic performance and the environmental performance of this study. The economic indicator is the relative net present value (NPV_{rel}) used to analyse the project's profitability. All system in this study is considered to have a 20-year lifetime. The NPV_{rel} is compared with the reference system, which has the same electric, heating, and cooling system, and 8 E-boats have both boat-to-building and building-to-boat functions. The detailed Equation of NPV_{rel} is below:

$$NPV_{rel} = \sum_{n=1}^{20} \frac{(C_{subsidy,gen,n} + C_{imp,save,n})}{(1+i)^n} + SV_{EB} - \left(I_{WEC} + I_{FPV} + \sum_{n=1}^{20} \frac{C_{O\&M,n}}{(1+i)^n} + \sum_{j=1}^{20} \frac{C_{EB,replacement,j}}{(1+i)^j}\right) \quad (10)$$

where the "$C_{subsidy,gen,n}$" is the subsidy received for renewable energy generation (after inverter) during the year "n", the "n" total life span is considered as 20 years. "$C_{imp,save,n}$" is the saved electricity fee compared to the reference system. The reference system is assumed to import all electricity from the grid. "i" is the annual interest rate, considered as 2.139% per annum based on the average interest rate value for Hong Kong for the previous five years (from 2015 to 2019) from the World Bank (Bank). "SV_{EB}" is the salvage value of batteries of the E-boats. "I_{WEC}", "I_{FPV}" are the initial capital cost of the wave energy converter and floating photovoltaic, respectively. "$C_{O\&M,n}$" stands for the operation and maintenance cost of WEC and FPV within the year "n". "$C_{EB,replacement,j}$" is the total replacement cost of the boat batteries in year "j". The specific year for battery replacement is calculated based on the number of charges and discharge cycles the battery undergoes per year; in this study, the battery is replaced once the accumulated total number of cycles exceeds 2000 (SOELCAT 12, 2022). A detailed cost profile of the ocean renewable energy hybrid system, boat PV, batteries, and feed-in tariff is listed.

The last indicator concerning the environmental aspect is the annual operational equivalent CO_2 emissions of the system, "CE_a" is expressed in Eq. (11), "CE_p" (12) and "CE_{op}" (13) are the operational equivalent CO_2 emissions during the peak and off-peak period :

$$CE_a = \left(E_{imp,a} - E_{exp,a}\right) \cdot CEF_{eg} \quad (11)$$

$$CE_p = \left(E_{imp,p} - E_{exp,p}\right) \cdot CEF_{eg} \quad (12)$$

$$CE_{op} = \left(E_{imp,op} - E_{exp,op}\right) \cdot CEF_{eg} \quad (13)$$

where "$E_{imp,a}$" and "$E_{exp,a}$" are the annual import and export of electric energy to and from the grid. Therefore, "$E_{imp,p}$", "$E_{imp,op}$", "$E_{exp,p}$" and "$E_{exp,op}$" are the import and export of electric energy to and from the grid during the peak and off-peak period. "CEF_{eg}" is the equivalent CO_2 emission factor of the local electric grid; this factor is considered 0.486 $kgCO_{2,eq}$/kWh in this study. Moreover, it concerns the five-year (2016–2020) average value of equivalent CO_2 emission factor reported by the Hong Kong power company, China Light and Power Company Syndicate (CLP) (CLP, 2020).

Table 5
The bulk tariff of electricity fee (CLP, 2021a).

Items				Charges
A	Monthly Demand Charge	On-Peak period[a]	Each of the first 650 kVA	68.4 (HKD/kVA)
			Each kVA above 650	65.4 (HKD/kVA)
		Off-Peak Period	Each off-peak kVA up to the on-peak billing demand	0 (HKD/kVA)
			Each off-peak kVA in excess of the on-peak billing demand	26.8 (HKD/kVA)
B	Monthly Energy Charge	On-Peak Period	Each of the first 200,000 units	0.753 (HKD/kWh)
			Each unit over 200,000	0.737 (HKD/kWh)
		Off-Peak Period	Each unit	0.676 (HKD/kWh)
C	Monthly Fuel Cost Adjustment			0.281 (HKD/kWh)

[a]Minimum on-peak billing demand is 100 kVA.

5. Simulation results, analyses and discussions

In this study, five main strategies are conducted for energy flexibility control, each strategy being a continuation of a non-dominated solution based on the results of the previous one. The simulation results for each strategy are investigated and analysed using the metrics presented in Section 4. To give a clear clue for this section, a flow chart of the research steps is shown in Fig. 10:

5.1. The tariff model and maximum flexibility potential of reference cases

5.1.1. Reference case 1

There are two reference cases in this study. Reference Case 1 only considers the demand for a hotel building with eight E-boats. Without renewable energy in the system, all the electric demand is supported by the grid only. The E-boats are active both in the building-to-boat and boat-to-building functions. This reference Case 1 is considered to calculate the saved electricity bill via applying flexibility control strategies and renewables. The tariff is based on the Hong Kong CLP commercial bulk tariff to calculate electricity bills (CLP, 2021a). The tariff is the aggregate of 3 items: Peak and off-peak demand charges, peak and off-peak energy charges, and fuel cost adjustment. Detailed costs for these three items are reported in Table 5.

In this study, all electricity charges are calculated based on the tariff model mentioned in Table 5, which consists of three items: Peak and off-peak demand charges, peak and off-peak energy charges, and fuel cost adjustments. Completely different from the off-peak period, the monthly demand charge during the on-peak period is 68.5 HKD/kVA up to 650 kVA, 65.4 HKD/kVA above 650 kVA. The off-peak demand charge is free when the off-peak demand is below the peak demand, and 26.8 HKD/kVA when the off-peak demand is higher than the peak demand. A restriction requires a minimum peak bill demand of 100 kVA, meaning that the minimum bill is always 100 kVA even if the maximum monthly peak demand is below 100 kVA or even 0. The monthly energy charges are also different for peak and off-peak periods, with the first 200,000 kWh during the peak period being charged at 0.753 HKD/kWh and 0.737HKD/kWh for the excess, and for off-peak, each unit is charged at 0.676 HKD. The last item is a monthly fuel cost adjustment of approximately 0.281 HKD/kWh. While the information on the feed-in-tariff is presented in Appendix B, it is still worth noting that the feed-in-tariff of CLP is calculated at 3 HKD/kWh based on the amount of total renewable energy generation. The energy exported to the grid has no extra revenue in this study.

Based on the bulk tariff calculation, when the grid only supports the hotel building and its 8 E-boats, the annual fee is around 1.12 million HKD. Fig. 11(a) reports the monthly electricity bill and maximum import power of reference Case 1. Monthly electricity bills remain around 80,000 HKD to 100,000 HKD, with November, December, and January to April being the lower months of the year and May to October almost always being around 100,000 HKD. Generally, the monthly energy charge is much larger than the monthly demand charge. In addition, the line graph shows that the monthly maximum import power is always greater during off-peak periods than peak periods, which results in an additional cost difference (26.8 HKD/kVA). The maximum monthly import power is approximately 230 to 285 kW in the off-peak period and 208 to 250 kW in the peak period. It is worth noting that the maximum import power is much higher during the off-peak period in January than in other months because of the need to fully charge the boat's batteries on the first day of January during the simulation.

5.1.2. Reference case 2

The second reference case equips the hybrid renewable system (20 units of WEC and 2726.3 m^2 of FPV) and keeps 8 E-boats. The E-boats follow the control strategies introduced in Section 3.2.1. In Fig. 11(b), compared with reference 1, there is a very significant drop in the monthly electricity bill. The generation of renewables helps save up to half the annual electricity fee, significantly reducing the energy charge of peak and off-peak periods. Reference 1 needs to pay 1.12 million HKD; however, reference 2 needs 0.55 million HKD. The annual saved electricity fee is about 0.57 million HKD without any energy flexibility control. Therefore, the imported energy and power data from reference 2 can be used as the baseline for regulation to estimate the maximum reduction in electricity charges. In the extreme case, assuming all peak power is reduced to zero and energy demand is shifted to off-peak periods, the total annual charge can be reduced by 28.7%. However, a special rule for monthly demand chargers is that even if peak power can be reduced to zero, the minimum peak billing demand is 100 kVA. Therefore, the maximum tariff reduction would be 13.9% if this mandatory limit is considered. In the following sub-sections, the proposed control strategy is improved step by step around shaving peaks and filling troughs to minimise annual electricity costs and increase the relative net present value.

5.2. The flexibility investigation of the coordination between the ocean energy charging and grid charging for the boat batteries

Section 3.2.2 has already introduced the final integrated flexibility control strategies of the E-boats. The following sub-sections investigate the detailed techno-economic-environmental performance of these strategies.

5.2.1. Strategy A: Adjust the working pattern of 8 E-boats

The original working pattern of the 8 E-boats was that they would cruise the waters together from 09:00 to 22:00 every day. Each cruise would last for 2 h, each cruise would last for half an hour, and the cruising distance would be 7.5 km, assuming

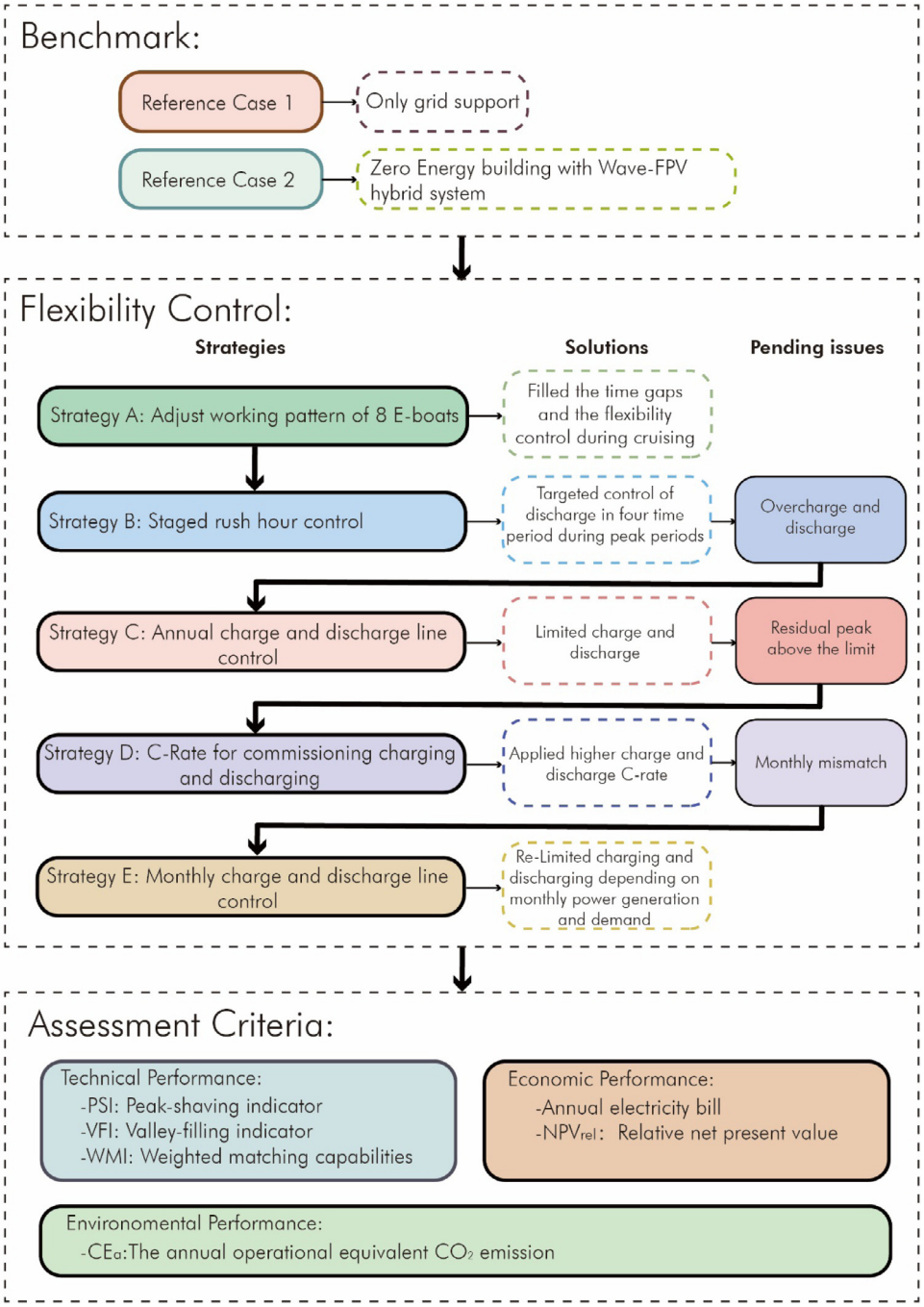

Fig. 10. The flow chart of the research steps, methodology, and assessment criteria.

that the cruising speed is maintained at 15 km/h. Based on this working schedule, there always have 30 min that the boats are disconnected from the building. During the 30 min of cruising, the boats are not allowed to discharge the batteries to support the building, leading it difficult for the E-boats to help shave the peak power. During this 30-min offshore working time, there may still be a maximum demand power for the month that has not been removed, and the demand charge for Part A for that month would not be reduced.

Strategy A for flexibility control ensures that boats are always available to support the hotel, as described in Section 3.2.2 and Fig. 6. The eight boats are split into two groups, and a new cross-working schedule is introduced to address this 30-min gap time issue. Fig. 12(a) shows the duration curve of the peak period to investigate the peak shaving capacity; there are two average lines to evaluate the PSI in this study. One is the "$P_{average,ref,p}$", which is 30 kW. This is the average import power value during the peak period (3756 h). Another one is the "$P_{average,ref,p}(100)$", which is 100 kW. This reference line was set up to consider the fact that the limit on the demand charge of the CLP bulk tariff is 100 kVA. Correspondingly, there are two valley-filling limit lines for the off-peak: "$P_{average,ref,op}$", which is 55 kW. Another is "$P_{average,ref,op}(100)$ ", 30 kW.

Fig. 12 shows the during curve of reference Case 2 and strategy A in the peak and off-peak periods. Comparing the red dash line with the grey area in Fig. 12(a) shows the positive impact on peak shaving. Although there is little change in peak power in the 250 kW to 100 kW range, a trend towards cuts can be seen in

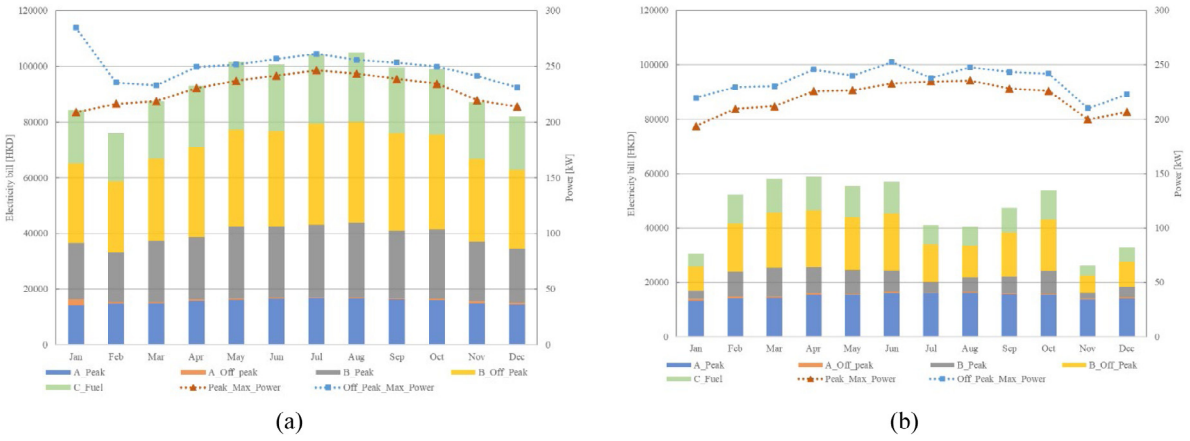

Fig. 11. The monthly electricity bill and maximum import power of reference Case 1 (Left) and 2 (Right). (A_peak: the demand charge of the peak period; A_Off_Peak: the demand charge of the off-peak period; B_Peak: the energy charge of the peak period; B_Off_Peak: the energy charge of the off-peak period; C_fuel: the fuel cost adjustment; Peak_Max_Power: the maximum import power of peak period; Off_Peak_Max_Power: the maximum import power of off-peak period)

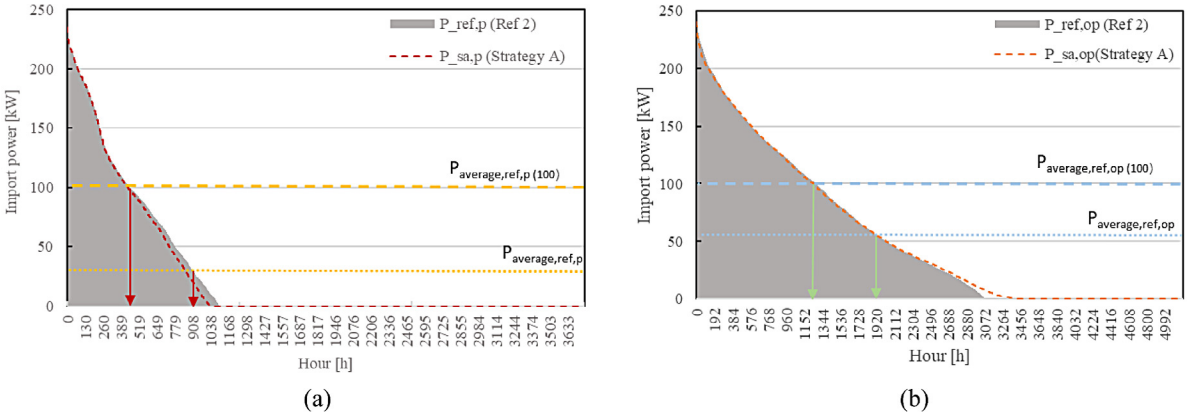

Fig. 12. The duration curve for peak-shaving (a) and valley-filling (b) capacity investigation during peak and off-peak periods with Strategy A.

Table 6
The investigation of techno-economic-environmental indicators for reference cases and strategy A.

Key Indicator	Energy flexibility capacity				Renewable matching capability			Economic indicator (without 100 kVA limit)		CO_2 emission ($kgCO_{2,eq}/m^2.a$)		
	PSI_p (100 kW)	VFI_{op} (100 kW)	PSI_p (30 kW)	VFI_{op} (55 kW)	WMI (annual)	WMI_p	WMI_{op}	Annual electricity bill (HKD)	NPV_{rel} (Million HKD)	CE_a	CE_p	CE_{op}
Ref 1	n.a.	n.a.	n.a.	n.a.	n.a.	n.a.	n.a.	1119741	0	118.58	46.54	72.04
Ref 2	0.00%	0.00%	0.00%	0.00%	0.671	0.701	0.641	554341	5.628	12.00	−14.22	26.20
Str A	2.32%	0.92%	0.80%	2.34%	0.674	0.708	0.640	547458	5.650	11.95	−14.57	26.51

the part below 100 kW. Similarly, Fig. 12(b) illustrates the valley-filling result during the off-peak period. It could check the orange dot line and the grey area; strategy A also takes a little effort to fill the power valley from 25 kW to 0 kW. The exact values can be found in Table 6. When the PSI_p limit line is 100 kW and 30 kW, the PSI of Strategy A is 2.32% and 0.8%, respectively. The lower the line means that more peak needs to be shaved. Therefore, the PSI is smaller. The corresponding VFI is 0.8% and 2.34% when the VFI_{op} limit line is 100 kW and 55 kW. The lower the limit line, the smaller the valley area; hence, the higher the VFI.

Table 6 reports other essential indicators to show the improvement and positive impact of Strategy A. It could be known that only by having this cross-schedule of these E-boats does the annual WMI still have an increase. In particular, the WMI is higher at peak times. It indicates that the adjustment of the boat travel plan is more prominent in enhancing energy matching during peak periods than off-peak periods. The economic part also reports a reduction in annual electricity fees (1.24%) and an improvement in relative NPV (0.39%). At the same time, this strategy has a small positive effect on emissions. The benefits of WMI are positively correlated with carbon emissions during the peak period, even to the extent that carbon emissions can be negative, meaning that less electricity is imported than renewable energy is exported during the peak period. Of course, the cost of increased interaction between E-boats and buildings is reflected in the off-peak period. As a result, the WMI is worse during the off-peak, and the CE_a is higher because of the increased reliance on the grid to charge the E-boats.

5.2.2. Strategy B: Staged rush hour control

In the previous control, the boat-to-building function would be activated whenever the FSOC of the battery was above 0.8 (mentioned in Section 3.2.2 Table 4). This rough control did not have separate controls for the peak and off-peak periods. Based

Table 7
Staged discharge plan for 4 periods during the peak period. (Bold and underlined point Case B3 has the best economic performance).

Cases			Lower FSOC for discharging									
			A	B1	B2	**B3**	B4	B5	B6	B7	B8	B9
Staged discharge period	A team	9:00-12:00	0.8	0.7	0.7	**0.7**	0.6	0.6	0.6	0.5	0.5	0.5
		12:00-15:00	0.8	0.6	0.6	**0.6**	0.5	0.5	0.5	0.4	0.4	0.4
		15:00-18:00	0.8	0.5	0.5	**0.5**	0.4	0.4	0.4	0.3	0.3	0.3
		18:00-21:00	0.8	0.25	0.25	**0.25**	0.25	0.25	0.25	0.25	0.25	0.25
	B team	9:00-12:00	0.8	0.65	0.55	**0.45**	0.65	0.55	0.45	0.65	0.55	0.45
		12:00-15:00	0.8	0.55	0.45	**0.35**	0.55	0.45	0.35	0.55	0.45	0.35
		15:00-18:00	0.8	0.45	0.35	**0.25**	0.45	0.35	0.25	0.45	0.35	0.25
		18:00-21:00	0.8	0.25	0.25	**0.25**	0.25	0.25	0.25	0.25	0.25	0.25

on the new electricity business model, it can be observed that, even after equipping renewables, the demand charge during the peak period still accounts for about 1/3 of the monthly electricity bill. Therefore, the new control strategy should react to how these maximum peak powers are eliminated. In Strategy B, the first consideration was to specify a staged discharge plan, specifying that the boat battery could be discharged to a constant level (e.g. 0.3). This constant FSOC control would result in the boat running out of power during the peak period and being unable to continue with the remaining tourist activities. Moreover, in the old control, the lower FSOC was reduced to a maximum of 0.3. In the next strategy, it is considered that the boat battery can be discharged to 0.2, which provides more discharging potential to support energy flexibility control.

Strategy B investigates nine discharge schedules to ensure that the E-boat can perform its cruising activities properly while providing as much energy as possible to the building. First, Table 7 divides the peak period (9:00 to 21:00) into four sections. Depending on the power demand of the hotel, we can see that the two periods between 9:00 and 12:00 and 18:00 and 21:00 are the morning and evening peak periods of the building, respectively. These two periods require more E-boat support than the two periods between 12:00 and 18:00; otherwise, the building would rely on the grid. Therefore, Strategy B is expected to control the boat with different discharge constraints at different periods. Nine cases of discharge schedules are reported below; both E-boats fleets limit their lower FSOC at 0.25, considering there have night tourist activities after 21:00. The real lower FSOC for discharging is 0.2.

Fig. 13 shows the economic performance of Strategy B with 9 different cases; B3 has the highest relative NPV (4.987 million HKD) and the lowest annual electricity bill (532,109 HKD). The reason is that when applying the B3 discharge schedule, A team boats could retain most of their power at three periods of the day, mainly discharge between 18:00 and 21:00. In contrast, B team boats discharge more intensively between 09:00 and 12:00 in the morning. With this staggering discharge strategy, electricity bills are naturally reduced when the morning and evening peaks have been shaved as far as possible.

It is worth noting that with the adoption of Strategy B3, the annual electricity bill has dropped from 547,457 HKD (Strategy A) to 532,109 HKD. However, the relative NPV has dropped from 5.65 million HKD (Strategy A) to 4.987 million HKD. Since the E-boats are frequently charged and discharged to provide energy support for the building, increasing their consumption. Whereas in Strategy A, the batteries of both fleets only needed to be replaced in years 15 and 18. In Strategy B, A team boats need to be replaced in years 8 and 16, and B team boats need to be replaced in year 12. Therefore, an earlier and more time battery replacement does not offer an NPV advantage for Strategy B3.

Due to the intense interaction between E-boats and building with Strategy B3, the PSI with a 100 kW limit could achieve 159.54%. It is worth noting that when the PSI exceeds 100%, the amount of peak shaving exceeds what is needed. It brings two

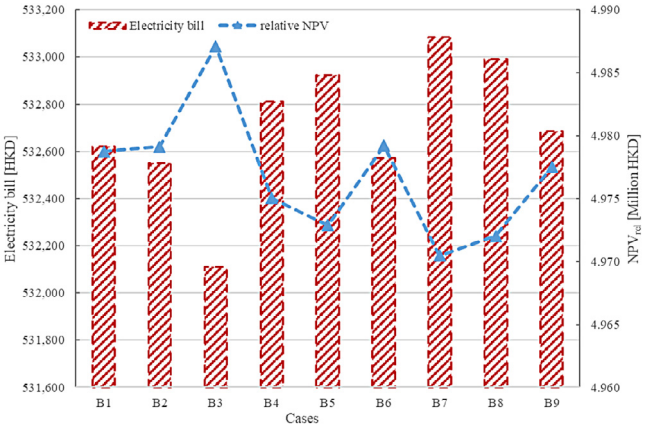

Fig. 13. Annual electricity bill and relative NPV of nine cases with Strategy B.

problems: increased wear and tear on the battery, as mentioned before, and an earlier year for replacement, resulting in higher costs. Second, if the local utility company rules that if the import power is under 100 kW, it still has to pay a minimum demand charge of 100 kW, this excess does not benefit. However, when the PSI limit line drops to 30 kW, more shaving is required, and at this point, Strategy B3 can only reach 54.98%. At the same time, Strategy B3 achieves a valley-filling of 20.04% and 32.69% at 100 kW and 55 kW limit lines, respectively (see Fig. 14). Table 8 also reports the improvement of annual WMI and WMI_p and the negative impact of WMI_{op} and CO_2 emission because of the overuse of batteries during the peak period; there is an increased reliance on the off-peak period grid to charge the boat.

In Strategy B, although the annual fee has decreased, the relative NPV has not increased due to the unreasonable and excessive use of batteries. One important reason is that the frequency of battery replacement has increased due to the excessive use of batteries. Therefore, although only the cycle-life-based degradation of the battery is considered, this model still has sufficient impact for this article. However, it is clear that a more comprehensive model of battery degradation will need to be refined in future work and incorporated into the observations of optimisation-based control.

5.2.3. Strategy C: Annual charge and discharge line control

Based on strategy B, it could be noticed that there is still some very high import power, and the presence of these peaks dominates the cost of the demand charge for specific months. In addition, it is found that to eliminate as many peaks as possible, the VFI, although boosted, also sees that the off-peak weights can be higher than the average line of imports. Therefore, based on the above learning, limiting the annual charge and discharge is necessary to avoid over-charging and over-discharging. Strategy C continues to observe 30 cases of annual charging and discharging lines based on Strategy B3. The charge limit line changes from

Table 8
The investigation of techno-economic-environmental indicators for strategy A and strategy B3.

Key Indicator	Energy flexibility capacity				Renewable matching capability			Economic indicator (without 100 kVA limit)		CO_2 emission (kgCO $_{2,eq}$/m^2.a)		
	PSI_p (100 kW)	VFI_{op} (100 kW)	PSI_p (30 kW)	VFI_{op} (55 kW)	WMI (annual)	WMI_p	WMI_{op}	Annual electricity bill (HKD)	NPV_{rel} (Million HKD)	CE_a	CE_p	CE_{op}
Str A	2.32%	0.92%	0.80%	2.34%	0.674	0.708	0.640	547,458	5.650	11.95	−14.57	26.51
Str B3	159.54%	20.04%	54.98%	32.69%	0.677	0.790	0.572	532,109	4.987	13.46	−22.89	36.34

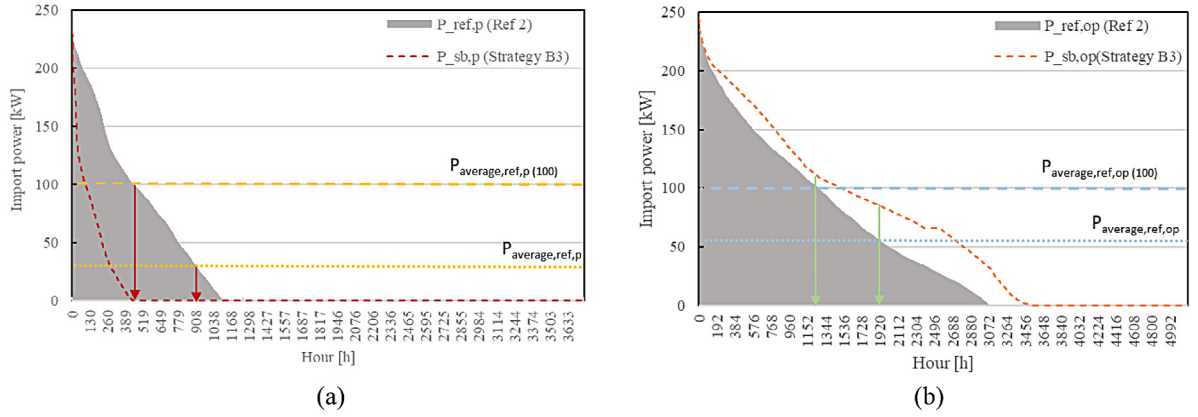

Fig. 14. The duration curve for peak-shaving (a) and valley-filling (b) capacity investigation during peak and off-peak periods with Strategy B.

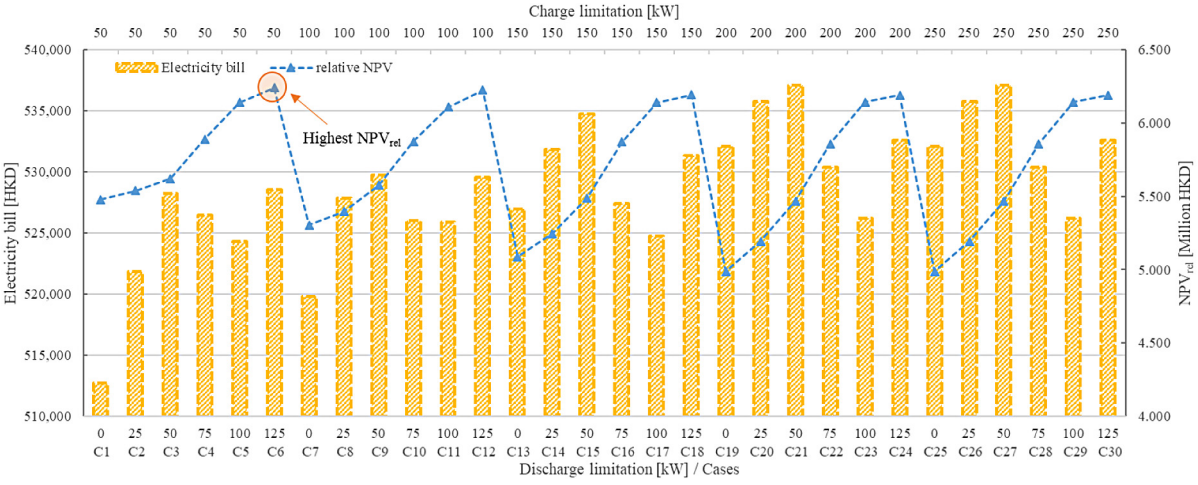

Fig. 15. The annual electricity bill and relative NPV of 30 cases with Strategy C.

50 kW to 250 kW, with each group increasing by 50 kW, making a total of 5 cases, and the discharge limit line changes from 0 kW to 125 kW, with each group increasing by 25 kW, making a total of 6 cases. The different charge and discharge lines would then be combined into 30 cases.

Fig. 15 illustrates the annual electricity bill and relative NPV of 30 cases with different annual charging and discharging limitation. It could be noticed that the electricity bill does not show a direct negative correlation with NPV_{rel}; the case of C1 has the cheapest annual electricity bill; however, its NPV_{rel} is not the highest. Instead, the best NPV_{rel} is found in C6, which has an annual electricity bill of approximately 528,549 HKD and a relative NPV of 6.240 million HKD. In addition, when the charge line is fixed, the higher discharge line has a higher relative NPV (e.g., Cases C1 to C6). Similarly, when the discharge line is fixed, the lower charge line has a higher relative NPV. It is because a lower discharge line and a higher charge line results in more battery consumption, which is reflected in the replacement cost of the battery. Therefore, although C6 does not have the lowest annual electricity cost, it avoids not having too much charging and discharging interaction and improves the overall relative NPV of the hybrid system.

Looking at Fig. 16(a), with the adoption of Strategy C6, most peak power is reduced to less than 125 kW, and their PSI is 58.85% and 20.28% when the PSI limit line is 100 kW and 30 kW, respectively. At the same time, the valley-filling has also improved considerably, avoiding overcharging while at the same time valley-filling. 12.71% and 22.98% VFI can be achieved with a limit line of 100 kW and 30 kW, respectively, as reported in Table 9.

By comparing B3 and C6, it can be seen that based on the current total battery capacity (supported by eight electric boats), it is not the case that discharging the battery as much as possible to have a lower annual charge and higher PSI and VFI result in a higher NPV. Therefore, the reduction in PSI, VFI, and annual WMI occur, but with the benefit that the C6 has a lower electricity bill and carbon emissions and a higher NPV than the B3.

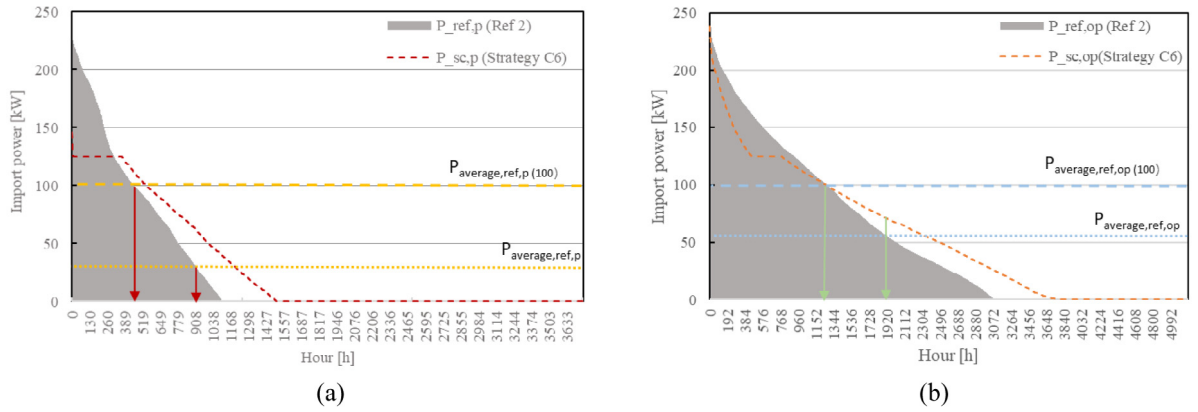

Fig. 16. The duration curve for peak-shaving (a) and valley-filling (b) capacity investigation during peak and off-peak periods with Strategy C.

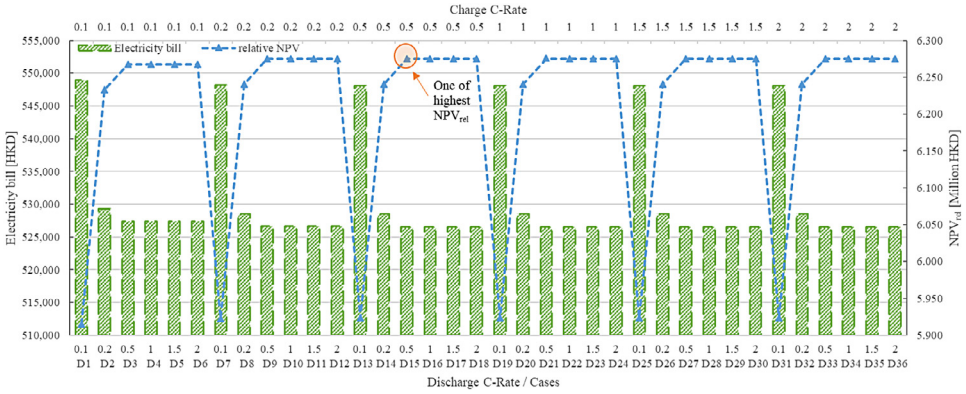

Fig. 17. The annual electricity bill and relative NPV with different combinations of charge and discharge C-Rate.

Table 9
The investigation of techno-economic-environmental indicators for strategy B3 and strategy C6.

Key Indicator	Energy flexibility capacity				Renewable matching capability			Economic indicator (without 100 kVA limit)		CO_2 emission ($kgCO_{2,eq}/m^2.a$)		
	PSI_p (100 kW)	VFI_{op} (100 kW)	PSI_p (30 kW)	VFI_{op} (55 kW)	WMI (annual)	WMI_p	WMI_{op}	Annual electricity bill (HKD)	NPV_{rel} (Million HKD)	CE_a	CE_p	CE_{op}
Str B3	159.54%	20.04%	54.98%	32.69%	0.677	0.790	0.572	532,109	4.987	13.46	−22.89	36.34
Str C6	58.85%	12.71%	20.28%	22.98%	0.649	0.685	0.608	528,549	6.240	12.46	−14.04	26.50

5.2.4. Strategy D: C-Rate for commissioning, charging and discharging

Based on the investigation of Strategy C, even though the annual discharge line goes to 125 kW, there are still some peaks above this limitation. The obstacle could be the C-Rate of discharge and charge. The C-rate measures the rate at which a battery is charged or discharged (Team, 2008). The 1C means the discharge current would discharge the entire battery in 1 h. This sub-section will investigate 36 cases with different charging and discharging C-rate. There are 6 options of C-Rate of charge, they are 0.1C, 0.2C, 0.5C, 1C, 1.5C and 2C. The options for discharge are the same. Fig. 17 illustrates the economic performance with different charge and discharge C-Rate combinations.

Fig. 17 shows that when the charge rate is fixed, a higher discharge rate could bring lower electricity fees and higher relative NPV. However, the further benefit would stop when the discharge C-rate is 0.5C. Considering that the total energy capacity that could be discharged from the boat battery is limited, the higher C-rate beyond 0.5C would not further help to shave the peak. Similarly, when the discharge C-rate is fixed, the higher charge C-rate helps reduce the annual electricity fee and increase the relative NPV, and the highest point of NPV stops at 0.5C of charge. Case D15 is one of the best charging and discharging C-rate combinations, and then D16, D17, D18, D22, and D23. A charge and discharge C-rate of 0.5C was chosen, considering that using a higher C-rate would be detrimental to the battery's life cycle.

Table 10 reports the key indicators of the hybrid system with strategies C6 and D15. After increasing the charge and discharge C-rate from 0.2C (in strategy C6) to 0.5C (in strategy D15), the PSI and VFI slightly improved. The better performance could be found in the annual electricity bill, reduced from 528,549 to 526,564 HKD, and the increase of relative NPV from 6.240 million HKD to 6.276 million HKD. The matching capabilities and CO_2 emissions remain virtually unchanged. The main reason for this unchanging is because there is a limit to the capacity that can be discharged from a boat's battery at each period, and the change and discharge in C-rate are also limited in terms of energy flexibility and matching capability.

To further reduce the electricity, 2 representative months present their maximum import power per time step in Fig. 18. As designed in the annual charge and discharge line, the maximum import power is expected not to exceed 125 kW during the peak period. However, this target is hard to achieve in April, partly because of the increased demand for electricity and partly because

Table 10
The investigation of techno-economic-environmental indicators for strategy C6 and strategy D15.

Key Indicator	Energy flexibility capacity				Renewable matching capability			Economic indicator (without 100 kVA limit)		CO_2 emission (kg$CO_{2,eq}$/m^2.a)		
	PSI_p (100 kW)	VFI_{op} (100 kW)	PSI_p (30 kW)	VFI_{op} (55 kW)	WMI (annual)	WMI_p	WMI_{op}	Annual electricity bill (HKD)	NPV_{rel} (Million HKD)	CE_a	CE_p	CE_{op}
Str C6	58.85%	12.71%	20.28%	22.98%	0.649	0.685	0.608	528,549	6.240	12.46	−14.04	26.50
Str D15	58.96%	12.70%	20.32%	22.96%	0.649	0.685	0.608	526,564	6.276	12.46	−14.04	26.50

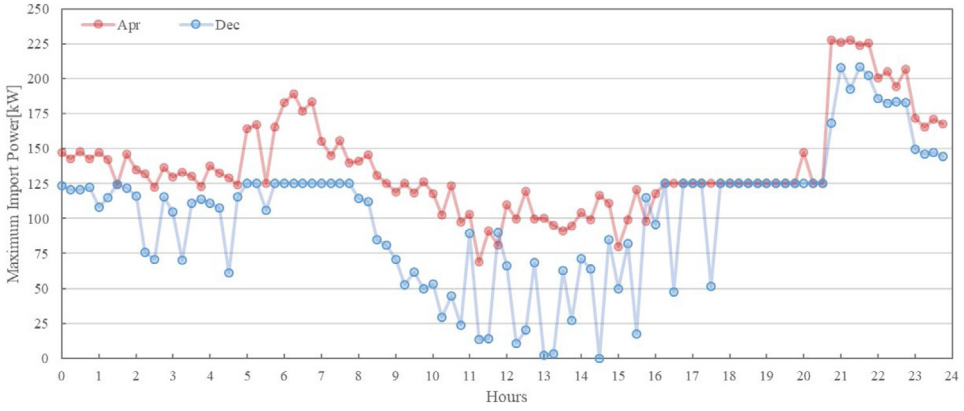

Fig. 18. The maximum import power per time step of April and December.

renewable generation in April does not support most of the peak period. A peak cannot be chipped away at 20:00 to 21:00, around 150 kW, determining the peak demand charge bill in April. A better charge plan for this month should be reorganised based on the generation characteristics of this month to shave the last peak. Another issue occurred in December; there are many valleys during the peak period from 9:00 to 16:00. However, the annual discharge line is 125 kW, limiting further shaving considering the excellent performance of generation in December. The specific control strategy should be improved monthly for the different demands and generations.

5.2.5. Strategy E: Monthly Charge and discharge line control

Based on the study and investigation of Strategy D, it could be noticed that different months have different generation and energy needs; the annual line control limits the ability for further flexibility in certain months. Therefore, in this sub-section, the monthly control will be conducted. Similarly, as the annual control, the monthly charging limit lines change from 50 kW to 250 kW, with an increase of 50 kW per case, for a total of 5 cases, and the monthly discharge limit lines change from 0 kW to 125 kW, with an increase of 25 kW per case, for a total of 6 cases. The different charging and discharging lines are combined to ultimately 30 cases per month, 360 cases for a one-year simulation. The final monthly charge and discharge line is reported below in Fig. 19; each monthly line could re-match a better charge and discharge limitation with its monthly generation. Strategy E would bring a significant reduction in annual operation fees. As shown in Fig. 19, the dashed areas report the final charge and discharge line for each month. The dot lines illustrate the monthly maximum import power concerning the limit line for peak and off-peak periods.

Fig. 19 reports that the maximum monthly import power is almost close to the designed limited discharge line, with higher values only in March, July and September. Conversely, the maximum import power during off-peak hours is difficult to achieve at the design charge line. The reason is that the hotel building has a significant energy demand between 21:00 and 00:00, and the E-boat batteries have run out and cannot support the discharge. The lower charge line could help limit the non-cost-effective grid charge.

Fig. 20 shows the duration curve with Strategy E. The significant peak shaving achievement is presented in Fig. 20; it could be known that the import power is reduced stepwise, the duration curve matches the monthly discharge line, and the remaining peak is serval hours from 125 kW to 100 kW. As shown in Table 11, PSI_p (100 kW) can reach 98.01% with strategy E, and PSI_p (30 kW) is significantly increased to 33.78%. The annual line for charging in Strategy C is only 50 kW; in Strategy E, the monthly charge line would increase if more grid charges could earn more cost-effective discharge during the night. Fig. 19 shows that the effect is noticeable when the charge line is increased to 150 kW in January, and the discharge line is finally peak shaving at a perfect 0 kW. It also results in certain sacrifices, mainly in the form of a weaker valley-filling effect during the off-peak period of this month. Therefore, the VFI_{op} (100 kW) and VFI_{op} (55 kW) are improved to 17.05% and 31.51%, respectively.

Meanwhile, Table 11 shows that Strategy E has also helped improve the WMI, with the annual WMI rising back to 0.666 and WMI_p rising significantly to 0.725. However, WMI_{op} has fallen slightly due to the need to discharge as much as possible to the limited discharge line during the peak period. The discharge line is more dependent on the grid in the off-peak period. In addition, the higher ability of peak power shaving positively affects the reduction in annual electricity bills. By applying the monthly control, the annual bill could reduce to 486,012 HKD, a reduction of 12.22% compared to reference Case 2. The relative NPV improved to 6.563 million HKD, roughly 16.62% compared to reference Case 2. It is worth mentioning that although the techno-economic-environmental performance is better in the peak period, this is at the expense of the off-peak period performance, so it can be seen that the CE_{op} rises to 29.67 kg$CO_{2,eq}$/m^2.a and affects CE_a, so that annual emission goes to 12.98 kg$CO_{2,eq}$/m^2.a

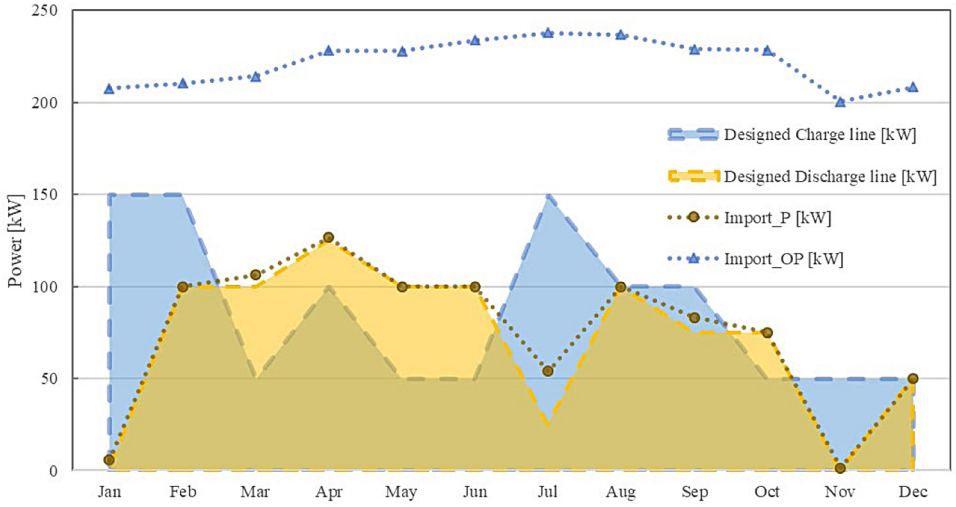

Fig. 19. The designed monthly charge and discharge line in Strategy E and maximum import power during peak and off-peak periods.

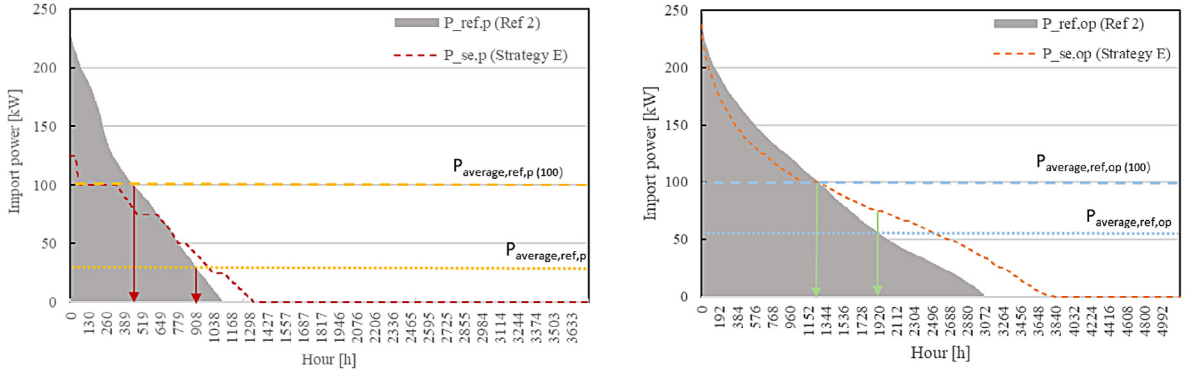

Fig. 20. The duration curve for peak-shaving (a) and valley-filling (b) capacity investigation during peak and off-peak periods with Strategy E.

Table 11
The investigation of techno-economic-environmental indicators for strategy D15 and strategy E.

Key Indicator	Energy flexibility capacity				Renewable matching capability			Economic indicator (without 100 kVA limit)		CO_2 emission ($kgCO_{2,eq}/m^2.a$)		
	PSI_p (100 kW)	VFI_{op} (100 kW)	PSI_p (30 kW)	VFI_{op} (55 kW)	WMI (annual)	WMI_p	WMI_{op}	Annual electricity bill (HKD)	NPV_{rel} (Million HKD)	CE_a	CE_p	CE_{op}
Str D15	58.96%	12.70%	20.32%	22.96%	0.649	0.685	0.608	526,564	6.276	12.46	−14.04	26.50
Str E	98.01%	17.05%	33.78%	31.51%	0.666	0.725	0.606	486,012	6.563	12.98	−16.70	29.67

5.3. The economic sensitivity analysis of the utility business model and policy suggestion

5.3.1. Economic sensitivity analysis with and without 100 kVA limitation

This research is based on the utility business model of CLP, as mentioned in Table 5. The demand charge during the peak period has a 100 kVA limitation. When the maximum import power during the peak period is lower than 100 kVA, this part of the tariff still asks for 68.4 HKD/kVA for 100 kVA. This 100 kVA line affects the annual bill when the flexibility control shaves the import power. Therefore, in this sub-section, the annual operational bill of 2 reference cases and 5 main flexibility control strategies are investigated with and without taking the 100 kVA into account.

The bar chart in Fig. 21 reports the composition of the annual electricity bill for the hotel building equipped with the Wave-FPV renewable energy system. It can be seen that the demand charge during the peak period is significantly reduced with the adoption of more refined flexibility control (from Strategy A to Strategy E). Meanwhile, the demand charge during the off-peak period increases, considering that the tariff model requires payment for the portion of the off-peak that is greater than the peak period. The line chart in Fig. 21 and Table 12 compare the annual electricity bill of different cases with and without considering the 100 kVA line. It can be known that only Strategy E receives the most significant impact. Strategy B3 also has an impact. However, it is not very obvious. Strategy E has a discharge control for different months, and many months have enough potential to reduce the peak power to 100 kVA. Therefore, if this 100 kVA line is higher than the minimum power that can be shaved in corresponding flexibility control, this line significantly limits the economic effect of flexibility control.

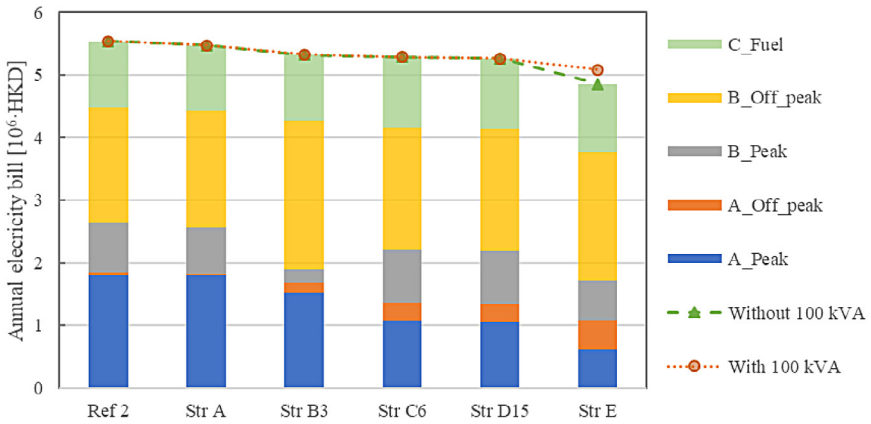

Fig. 21. The annual electricity bill with and without considering 100 kVA line limitation for reference Case 2 and 5 strategies.

Table 12
The annual electricity bill with and without considering the 100 kVA line limitation.

Annual electricity bill [HKD]	Ref 1	Ref 2	Str A	Str B3	Str C6	Str D15	Str E
Without 100 kVA	1,119,741	554,341	547,458	532,109	528,549	526,564	486,012
With 100 kVA	1,119,741	554,341	547,458	532,770	528,549	526,564	508,643

5.3.2. Economic sensitivity analysis of five sections of tariff

The CLP reported that in September 2021, the Average Net Tariff in 2022 was 128.9 cents per unit of electricity, equivalent to an upward adjustment of 5.8%. The adjusted tariff takes effect on January 2022. The central affected part of the tariff is the fuel cost adjustment. It reported an increase from 28.1 to 38.6 cents per unit (CLP, 2021a, 2022). The coal price keeps rising, resulting in another increase in fuel cost to 39.7 cents/unit in March 2022. However, this study considers an annual energy escalation ratio is around 1.313% (Census and Statistics Department, 2020). This study does not discuss which of the five tariff components covered by the utility business model would significantly impact the annual electricity bill. Therefore, in this sub-section, it is assumed that the utility business model includes five charge components (the energy demand during the peak and off-peak period, the energy charge for both periods and the fuel adjustment cost) increases to 5%, respectively.

As shown in Table 13, the conventional hotel buildings, which rely on the grid for energy supply (Reference 1), are more sensitive to the rise or fall of energy charge and fuel adjustment fuel and less sensitive to the energy demand. When the cost of energy charge of the peak and off-peak period increases by 5%, which means an increase from 0.753 HKD/kWh and 0.676 HKD/kWh to 0.791 HKD/kWh and 0.710 HKD/kWh, respectively, they bring a 1.24% and 1.72% increase to the annual electricity bill. Fuel cost is second only to energy charge in terms of cost increase, which means that the grid-based system is most sensitive to the part about energy charge because of its vast energy demand. Therefore, the traditional building is recommended to equip a renewable energy system for power supply, significantly reducing the imported energy and the annual operational bill. Moreover, when the hotel is equipped with renewable energy (Reference 2), its annual generation equals its annual energy demand. However, the energy charge of the off-peak period still dominates the most sensitive part; it has significantly diminished the impact of the sensitivity of energy costs during peak periods and fuel costs. Instead, it is more sensitive to the demand charge of the peak period. In other words, when the demand charge of the peak period increases from 68.4 HKD/kVA to 78.8 HKD/kVA, the impact on the cost fluctuation of the annual electricity bill is 1.62%. It also indicates that for zero energy hotel building, flexibility control, weakening the maximum import power of peak period can be more effective in saving its annual bill.

At last, when Strategy E is adopted, the imported power during the peak period is shaved a lot by the integrated flexibility control, and noticeably, based on this control strategy, the annual electricity cost is no longer sensitive to the demand charge. However, the most significant impact is still the energy charge during the off-peak period, followed by the fuel cost. It also shows that the control strategy has successfully shifted the energy consumption from the peak to the off-peak period while shaving the power. Therefore, if the energy charge during the off-peak period increases by 5% in the following year, it impacts the annual electricity bill by 2.12%, and similarly, if the fuel cost increases by 5%, the annual electricity bill increases by 1.12%.

In summary, when the CLP tariff calculation model is still applied, the most significant impact is the 100 kVA line of demand charge during the peak period. Considering the line limits, the potential benefits of reducing the import power below 100 kVA. If the government or utility wants to encourage customers to conduct peak reductions during the peak period, the first step is to reduce or remove the limitation of the 100 kVA line. Moreover, the difference between energy demand during peak and off-peak periods could be widened. Even lowering the off-peak period energy charge or charging multiple time slots would encourage off-peak usage while controlling demand at different times of the day.

5.4. The comparison between existing control and flexibility control, and future applications

5.4.1. The comparison between existing and flexibility control

Conventional electric transport, building, and grid interactions have often been discussed in single or bi-directional interactions such as B2V, V2B, G2V, and V2G (The "V" stands for the vehicles that could be E-boats in the current study). Rarely have studies discussed interaction scenarios and considered both the peak and the trough of the building, as well as peak and trough shaving in demand power. Table 14 compares the implications of adopting existing and current flexibility control on the same hybrid ocean energy system.

Table 13
The increased annual electricity bill and percentage with 5% increase on different tariff sections.

	Increased tariff and percentage [HKD]					
	Original	A_Peak*105%	A_Off_peak*105%	B_Peak*105%	B_Off_peak*105%	C_Fuel*105%
Ref 1	1119741 (+0%)	1129141 (+0.84%)	1120081 (+0.03%)	1133584 (+1.24%)	1138980 (+1.72%)	1132904 (+1.18%)
Ref 2	554341 (+0%)	563336 (+1.62%)	554595 (+0.05%)	558268 (+0.71%)	563576 (+1.67%)	559645 (+0.96%)
Str E	486012 (+0%)	489097 (+0.63%)	488371 (+0.49%)	489145 (+0.64%)	496293 (+2.12%)	491454 (+1.12%)

Table 14
Comparison of the implications of adopting existing and flexibility control.

No.	1	2	3	4
Interaction mode	Only G2V	B2V with G2V	B2V, V2B with G2V	Flexibility control
Characteristics	Electric grid to charge E-boats directly	Only activate the building-to-boat function, the renewable energy supports the building first and then charges the boats	When the renewable energy is insufficient to support the building, the boat batteries could be discharged to cover the short	Conditional activation of the boat-to-building function at peak power period and reliance on grid charging at off-peak power period
Annual electricity fee [HKD]	1,119,741	580,868	554,341	486,012
Relative NPV [million HKD]	0	2.11	5.63	6.56
Pros	No need to purchase any renewable energy system, low initial investment costs; no interaction of the electric boat with the building, low battery life consumption	Electricity bills have been reduced; renewable surplus energy could be consumed before exporting to the grid	Effective reduction in annual bills, reduced exported energy and reduced imported energy, significantly increasing the relative NPV	Targeted reduction in demand power; guaranteed frequency of battery replacement; improved the relative NPV
Cons	Expensive annual electricity bills	Energy imports from the grid remain quite high	Batteries are replaced relatively frequently	The optimisation-based control should be considered in the next stage

(1) G2V interaction is the most traditional interaction mode, meaning an electrical beam is used to charge the boat. The advantage is most apparent considering that it does not need to be equipped with any renewable systems. Therefore, the initial investment costs are the cheapest. Furthermore, as there is no additional interaction between the grid and the e-boat, the batteries of the E-boats have a relatively low lifetime consumption compared to other modes. A fatal disadvantage is paying a very high annual electricity bill.

(2) B2V with G2V is also a standard interaction mode in most studies. In this mode, only the boat-to-building function is activated. Renewable energy first satisfy the building demand, and the rest of the surplus renewable energy would use to charge the boat battery. When the surplus renewable energy is insufficient to support the daily demand of the boat, the rest of the energy is imported from the grid. The advantage is that there is a significant reduction in the cost of electricity due to the use of surplus energy. The disadvantage is that the amount of electricity introduced from the grid is still relatively high.

(3) B2V, V2B with G2V is based on the interaction mode of (2) with the addition of a boat-to-building function. The boat can discharge the battery to support the building when renewable energy cannot meet the demand. The advantage is that the exported and imported energy to and from the grid is reduced due to the increased self-consumption of renewable energy. Therefore, the annual electricity bill is significantly reduced, and the relative NPV is increased. However, this corresponds to an increase in the frequency of battery replacement due to the significantly higher interaction between the boat and the building.

(4) Flexibility control is based on the interactive mode of (3). This control also limits the grid to the boat to be recharged at low peaks not to increase the off-peak power demand. The flexibility control reduces annual costs and excessive battery discharging, increasing relative NPV.

5.4.2. Future applications

Based on the discussion and comparison between the existing and flexible control, it is known that the simple or unrestricted use of mobile transport as a backup mobile power source for buildings or the grid is a strategy for the economic practicality of attrition. The methodology of this paper aims at controlling the distribution of renewable energy by using a limited amount of removable power (batteries of electric boats), with some constraints, to achieve a precise peak and valley reduction in the energy consumption of buildings and reduce the annual electricity bill, as well as the consumption of the batteries. On the other hand, from the point of view of the utility companies and the government, some encouragement or restriction can be achieved by improving the weighting of the existing tariff model.

Firstly, it is important that the building has a backup energy storage system that can support energy flexibility control. Secondly, based on the local tariff model, it is probably more important to reduce peak power than peak energy. Thirdly, If there are significant morning and evening peaks, phased discharges are more effective in reducing monthly peak power demand than one-off or unlimited discharges. Finally, where data on renewable energy and building demand is available for the past calendar year, it is possible to specify a detailed charge and discharge line for each month to limit overcharging and over-discharging of the battery; if detailed data is not available, only the annual charge and discharge line can be specified.

Table A.1
The design parameters and principles of the hotel building envelopes, insulation and services systems.

	Parameters	Values		Design principal	
Insulation (U-value, W/m^2.K)	External roof	0.345	Infiltration (h-1)	According to the guideline of the Performance-based (EMSD, 2007): When the ventilation is on, the infiltration is 0 h-1; When the ventilation in off, the infiltration is 0.306 h-1.	
	External wall	2.308			
	Window glazing	2.78			
	Ground floor layer with soil layer	0.609			
	Parameters	Values		Parameters	Values
Occupants	Number	19 occupants on each hotel floor (EMSD, 2007)	Ventilation	Ventilation Type	Mechanical supply and exhaust ventilation with return air mixing and rotary heat recovery.
				Total supply flow rate (h-1)	1.5 (when the fan is on)
	Activity level MET (Fanger, 1970):1.2			Fresh air ratio in the total supply air flow rate	0.475
				Ventilation schedule	Follow the ventilation schedule listed in (EMSD, 2007).
	Parameters	Values			
AHU cooling and AHU heating	AHU cooling method	7/12 °C cooling coil			
	AHU and Reheat heating method	Hydronic heating			
	In-blown supply air temperature T_{sup} (° C)	A function with respect to the exhausted indoor air temperature $T_{exh,indoor}$: (1) T_{sup} = 17 °C ($T_{exh,indoor} \geq 24$ °C); (2) T_{sup} = 21 °C ($Te_{xh,indoor} \leq 21$ °C); (3) T_{sup} linearly increases from 17 to 21 °C ($T_{exh,indoor}$ drops from 24 to 21 °C)			
	Sensible effectiveness of the rotary heat recovery device	0.85			
	Latent effectiveness of the rotary heat recovery device	0.5			
	Specific ventilation fan power (W/(m^3/s))	(1) Supply fan: 800; (2) Exhaust fan: 800			
	Parameters	Values		Parameters	Values
Space cooling	Type	15/17 °C hydronic chilled ceiling system	Space heating	Type	Electric heating
	Room air set point (° C)	24 °C for all thermal zones		Room air set point (° C)	21 °C for all thermal zones
	Cooling schedule	Follow the cooling schedule listed in (EMSD, 2007)		Heating schedule	Follow the heating schedule listed in (EMSD, 2007)
	Parameters	Values			
DHW heating	Set point (° C)	55			
	Daily consumption volume (m^3)	17.8			
	DHW Schedule	Follow the DHW schedule listed in the (EMSD, 2007)			

The economic sensitivity analysis is also conducted for the 100 kVA line and five sections of electricity tariff as reported in Section 5.3.2. The 100 kVA line in the tariff model limits the flexibility control when the system has the potential to reduce its maximum monthly import power below 100 kVA. If Strategy E considers a 100 kVA line, the final annual fee reduction is limited to 508,643 HKD, a loss of 4.66% of annual savings. If the government or utility companies want to encourage the customers to reduce the import power during the peak period, the 100 kVA line should be set lower in the future. When considering a 5% increase in the cost of each section of the tariff model, the most sensitive section is the off-peak energy charge, followed by fuel cost adjustment. When they are increased by 5% of the original price, in Strategy E, the annual electricity bill increases by 2.12% and 1.12%, respectively. It also indicates that reducing the off-peak energy charge could more effectively encourage the customer to conduct flexibility control from peak to off-peak.

6. Conclusions

More and more efficient renewable energy systems and various energy interactions have been proposed in the literature to explore further and improve energy matching capabilities and energy flexibility. The popularity of electric transport has led to more research and attention to the interaction between electric transport and the electric grid. It has proven feasible to consider electric mobility as a mobile battery and use it to help peak-shaving and valley-filling and enhance better energy management systems. However, most existing studies focus on solar or wind energy, and electric vehicles have drawn more attention. This paper proposes an integrated energy flexibility control strategy to help the hotel building enhance peak-shaving and valley-filling capabilities. Eight electric boats and a hybrid WEC-FPV renewable energy system support the target hotel building. As a

Table B.1
The cost profile of the ocean renewable energy hybrid system, boat PV and battery, relative tariff, exchange rate, and energy escalation ratio.

Item	WEC (Wave dragon 1.5 MW, 2015)	FPV (Martins, 2019)	Boat PV (NREL, 2021)	Boat battery (Hsieh et al., 2019)
Initial Cost	45,630 HKD/kW	26,520 HKD/kW	37,331 HKD/kW	1,560 HKD/kWh
O&M Cost	4.80%	1.92%	0.86%	N.A.
Feed-in-tariff	3.00 HKD/kWh (CLP, 2021b)			
Interest Rate	2.139% (Worldbank, 2022a)			
USD to HKD exchange rate	7.8 (Worldbank, 2022b)			
Energy escalation ratio	1.313% (Census and Statistics Department, 2020)			

result, a comprehensive techno-economic-environmental investigation and analysis of the simulation results are presented. Moreover, two new indicators of peak-shaving (PSI) and valley-filling (VFI) are proposed to illustrate the peak-shaving and valley-filling capabilities of the hybrid system.

Five flexibility control strategies are investigated in this study, and each strategy adopts the non-dominant solution of the previous strategy. Therefore, strategy E is the final solution of this study. In Strategy E, different discharge and charge lines are set for each month according to the different monthly generation and demand characteristics. Therefore, the maximum import power in that specific month can be reduced as much as possible within its possible discharge range. The results are remarkable, and this final strategy resulted in a direct reduction of the annual fee to 486,012 HKD, a 12.22% reduction compared to reference Case 2. The relative NPV reaches 6.563 million HKD, about 16.62% higher than reference Case 2. PSI and VFI can reach 98.01% and 17.05% for a 100 kW line. It also indicates that only about 2% of the imported power is above 100 kW during the peak period is challenging to be shaved. The annual WMI decreases slightly from 0.671 in reference Case 2 to 0.666, and the CE_a also increases from 12.00 $kgCO_{2,eq}/m^2.a$ in reference Case 2 to 12.98 $kgCO_{2,eq}/m^2.a$. It is all because more off-peak grid charging must support the power and energy shaved during the peak period.

This study provides a comprehensive parametric study of several variables. The non-dominant results suggest that the variable most sensitive to flexibility control among the cases that have been studied may be the monthly discharge and charge limits of boat batteries. However, other variables (e.g. dynamic ageing issues of battery capacity) are not discussed and optimising the control and analysis should be future work to complement and update the conclusions and results of this paper.

CRediT authorship contribution statement

Xinman Guo: Methodology, Investigation, Writing – original draft, Writing – review & editing. **Haojie Luo:** Methodology, Investigation, Writing – original draft, Writing – review & editing. **Sunliang Cao:** Supervision, Funding acquisition, Project administration, Conceptualization, Methodology, Investigation, Writing – original draft, Writing – review & editing. **Yixing Lisa Gao:** Methodology, Funding acquisition, Investigation, Writing – original draft, Writing – review & editing. **Kai Pan:** Methodology, Funding acquisition, Investigation, Writing – original draft, Writing – review & editing.

Declaration of competing interest

The authors declare that they have no known competing financial interests or personal relationships that could have appeared to influence the work reported in this paper.

Data availability

Data will be made available on request.

Acknowledgements

This research is partially supported by the Project ID "P0033880" from Research Institute for Sustainable Urban Development (RISUD), and partially supported by the Project ID "P0039664" from Research Institute for Smart Energy (RISE), The Hong Kong Polytechnic University.

Appendix A

See Table A.1.

Appendix B

See Table B.1.

References

Ahmadi, M.M., Keyhani, A., Kalogirou, S.A., Lam, S.S., Peng, W., Tabatabaei, M., Aghbashlo, M., 2021. Net-zero exergoeconomic and exergoenvironmental building as new concepts for developing sustainable built environments. Energy Convers. Manage. 244, http://dx.doi.org/10.1016/j.enconman.2021.114418.

Ahmed, A., Ge, T., Peng, J., Yan, W.-C., Tee, B.T., You, S., 2022. Assessment of the renewable energy generation towards net-zero energy buildings: A review. Energy Build. 256, http://dx.doi.org/10.1016/j.enbuild.2021.111755.

Al-Bahrani, L.T., Horan, B., Seyedmahmoudian, M., Stojcevski, A., 2020. Dynamic economic emission dispatch with load dema nd management for the load demand of electric vehicles during crest shaving and valley filling in smart cities environment. Energy 195, http://dx.doi.org/10.1016/j.energy.2020.116946.

Al-Janahi, S.A., Ellabban, O., Al-Ghamdi, S.G., 2020. Technoeconomic feasibility study of grid-connected building-integrated photovoltaics system for clean electrification: A case study of Doha metro. Energy Rep. 6, 407–414. http://dx.doi.org/10.1016/j.egyr.2020.11.192.

Campana, P.E., Cioccolanti, L., François, B., Jurasz, J., Zhang, Y., Varini, M., Stridh, B., Yan, J., 2021. Li-ion batteries for peak shaving, price arbitrage, and photovoltaic self-consumption in commercial buildings: A Monte Carlo analysis. Energy Convers. Manage. 234, http://dx.doi.org/10.1016/j.enconman.2021.113889.

Cao, S.L., 2019. The impact of electric vehicles and mobile boundary expansions on the realization of zero-emission office buildings. Appl. Energy 251, http://dx.doi.org/10.1016/j.apenergy.2019.113347, ARTN113347.

Cao, S., Hasan, A., Sirén, K., 2013. On-site energy matching indices for buildings with energy conversion, storage and hybrid grid connections. Energy Build. 64, 423–438. http://dx.doi.org/10.1016/j.enbuild.2013.05.030.

Census and Statistics Department, 2020. Hong Kong energy statistics annual report. Retrieved from 920 https://www.censtatd.gov.hk/en/EIndexbySubject.html?pcode=B1100002&scode=90.

CLP, 2020. CLP sustainability report 2020.

CLP, 2021a. CLP 2021 electricity tariff tables. CLP Retrieved 2022/01/27 from https://www.clp.com.hk/content/dam/clphk/documents/customer-service-site/tariff-site/Tariff%20Table-English%20(2021-01-01).pdf.

CLP, 2021b. Tariff and Charges. https://www.clp.com.hk/en/customer-service/tariff.

CLP, 2022. CLP 2022 electricity tariff tables. Retrieved 03/31 from https://www.clp.com.hk/content/dam/clphk/documents/tariff-adjustment-2022/20211109_EN.pdf.

Corportation, I., 2014. Power generation using the kuroshio current. IHI Eng. Rev. 46, https://www.ihi.co.jp/var/ezwebin_site/storage/original/application/149ee9de3149aba2e1215fd5f9cd46ec.pdf.

EMSD, 2007. E. M. S. D. In: Performance-Based Building Energy Code. The Government of the Hong Kong Special Administrative Region.

Fanger, P.O., 1970. Thermal comfort. In: Analysis and Applications in Environmental Engineering. Danish Technical Press, Copenhagen, https://www.cabdirect.org/cabdirect/abstract/19722700268.

Feng, J., Yang, J., Wang, H., Wang, K., Ji, H., Yuan, J., Ma, Y., 2022. Flexible optimal scheduling of power system based on renewable energy and electric vehicles. Energy Rep. 8, 1414–1422. http://dx.doi.org/10.1016/j.egyr.2021.11.065.

FuturaSun, 2022.https://www.futurasun.com/en/.

Giouri, E.D., Tenpierik, M., Turrin, M., 2020. Zero energy potential of a high-rise office building in a mediterranean climate: Using multi-objective optimization to understand the impact of design decisions towards zero-energy high-rise buildings. Energy Build. 209, http://dx.doi.org/10.1016/j.enbuild.2019.109666.

Guo, X., Cao, S., Xu, Y., Zhu, X., 2021. The feasibility of using zero-emission electric boats to enhance the techno-economic performance of an ocean-energy-Supported Coastal hotel building. Energies 14 (24), http://dx.doi.org/10.3390/en14248465.

Hamza, M., Alsaadani, S., Fahmy, M., 2022. Exploring the potential of nearly zero energy retrofitting for generic office buildings in Cairo. Egypt. Energy Rep. 8, 116–122. http://dx.doi.org/10.1016/j.egyr.2022.01.089.

Hsieh, I.Y.L., Pan, M.S., Chiang, Y.-M., Green, W.H., 2019. Learning only buys you so much: Practical limits on battery price reduction. Appl. Energy 239, 218–224. http://dx.doi.org/10.1016/j.apenergy.2019.01.138.

Hsu, T.-W., Liau, J.-M., Liang, S.-J., Tzang, S.-Y., Doong, D.-J., 2015. Assessment of Kuroshio current power test site of green Island Taiwan. Renew. Energy 81, 853–863. http://dx.doi.org/10.1016/j.renene.2015.03.089.

Huang, M., He, W., Incecik, A., Cichon, A., Królczyk, G., Li, Z., 2021. Renewable energy storage and sustainable design of hybrid energy powered ships: A case study. J. Energy Storage 43, http://dx.doi.org/10.1016/j.est.2021.103266.

IEA, 2021a. Global EV outlook 2021. https://www.iea.org/reports/global-ev-outlook-2021?mode=overview.

IEA, 2021b. Net zero by 2050:A roadmap for the global energy sector. https://www.iea.org/reports/net-zero-by-2050.

IEA, 2021c. Ocean power. https://www.iea.org/reports/ocean-power.

IEA, 2021d. Renewable power. https://www.iea.org/reports/renewable-power.

IEA, 2021e. Tracking buildings 2021. https://www.iea.org/reports/tracking-buildings-2021.

iha, 2016. Technology case study: Sihwa lake tidal power station. https://www.hydropower.org/blog/technology-case-study-sihwa-lake-tidal-power-station.

Ioakimidis, C.S., Thomas, D., Rycerski, P., Genikomsakis, K.N., 2018. Peak shaving and valley filling of power consumption profile in non-residential buildings using an electric vehicle parking lot. Energy 148, 148–158. http://dx.doi.org/10.1016/j.energy.2018.01.128.

IRENA, 2020. Innovation outlook: Ocean energy technologies. Int. Renew. Energy Agency https://www.irena.org/-/media/Files/IRENA/Agency/Publication/2020/Dec/IRENA_Innovation_Outlook_Ocean_Energy_2020.pdf.

Kumar, G.M.S., Cao, S., 2021. Simulation-based techno-economic feasibility study on sector coupled net-zero/positive energy metro railway system in Hong Kong. Energy Convers. Manage. 248, http://dx.doi.org/10.1016/j.enconman.2021.114786.

Kumar, R., Waghmare, A., Nayak, S., Paswan, M., Achintya, 2021. Design of self sustainable zero energy building. Mater. Today: Proc. 46, 6737–6742. http://dx.doi.org/10.1016/j.matpr.2021.04.263.

Lan, L., Wood, K.L., Yuen, C., 2019. A holistic design approach for residential net-zero energy buildings: A case study in Singapore. Sustainable Cities Soc. 50, http://dx.doi.org/10.1016/j.scs.2019.101672.

LG, 2022.340 W NeON® 2 Black Solar Panel for Home https://www.lg.com/us/business/solar-panels/lg-lg340n1k-l5.

Li, M., Cao, S., Zhu, X., Xu, Y., 2022a. Techno-economic analysis of the transition towards the large-scale hybrid wind-tidal supported coastal zero-energy communities. Appl. Energy 316, http://dx.doi.org/10.1016/j.apenergy.2022.119118.

Li, M., Luo, H., Zhou, S., Senthil Kumar, G.M., Guo, X., Law, T.C., Cao, S., 2022. State-of-the-art review of the flexibility and feasibility of emerging offshore and coastal ocean energy technologies in east and southeast Asia. Renew. Sustain. Energy Rev. 162, http://dx.doi.org/10.1016/j.rser.2022.112404.

Li, C., Zhang, L., Ou, Z., Wang, Q., Zhou, D., Ma, J., 2022b. Robust model of electric vehicle charging station location considering renewable energy and storage equipment. Energy 238, http://dx.doi.org/10.1016/j.energy.2021.121713.

Luo, H., Cao, S., Lu, V.L., 2022. The techno-economic feasibility of a coastal zero-energy hotel building supported by the hybrid wind–wave energy system. Sustain. Energy Grids Netw. 30, http://dx.doi.org/10.1016/j.segan.2022.100650.

Ma, S.-C., Yi, B.-W., Fan, Y., 2022. Research on the valley-filling pricing for EV charging considering renewable power generation. Energy Econ. 106, http://dx.doi.org/10.1016/j.eneco.2021.105781.

Ma, J., Zhu, L., Shen, Y., Rong, X., Zhang, H., Yang, H., 2021. Demand response-based commercial mode and operation strategy of customer-side energy storage system. Energy Rep. 7, 1390–1399. http://dx.doi.org/10.1016/j.egyr.2021.09.123.

Madison, 2022. T. U. W. TRNSYS 17. Retrieved 03 from https://sel.me.wisc.edu/trnsys/features/.

Martins, B.P., 2019. Techno-economic evaluation of a floating PV system for a wastewater treatment facility. https://kth.diva-portal.org/smash/get/diva2:1332527/FULLTEXT01.pdf.

Meteonorm, 2022. Meteonorm. Retrieved 03/18 from https://meteonorm.com/en/.

NREL, 2021. Distributed Generation Energy Technology Capital Costs. https://www.nrel.gov/analysis/tech-cost-dg.html.

Observatory, H.K., 2020. Climate of Hong Kong. Retrieved 03/18 from https://www.hko.gov.hk/en/cis/climahk.htm.

Parmeggiani, S.C., Fernandez, Julia, Arthur, Pecher, Friis-Madsen, E., Sørensen, H.C., Kofoed, Jens Peter, 2011. Performance assessment of the wave dragon wave energy converter based on the equimar methodology.

SEM-REV, 2019. WAVEGEM®: the wave energy recovery prototype. 2019. https://sem-rev.ec-nantes.fr/english-version/devices-tested/wavegem%C2%AE-the-wave-energy-recovery-prototype.

She, C., Jia, R., Hu, B.-N., Zheng, Z.-K., Xu, Y.-P., Rodriguez, D., 2021. Life cycle cost and life cycle energy in zero-energy building by multi-objective optimization. Energy Rep. 7, 5612–5626. http://dx.doi.org/10.1016/j.egyr.2021.08.198.

SOELCAT 12, 2022.https://soelyachts.com/soelcat-12/.

Solar Energy Laboratory of the University of Wisconsin-Madison, T.E.G., 2017. CSTB – centre scientifique et technique du bâtiment. In: TESS – Thermal Energy Systems Specialists. Section 8.7 Meteonorm data. In (Vol. Volume 8 Weather Data).

Team, M.E.V., 2008. A guide to understanding battery specifications. https://web.mit.edu/evt/summary_battery_specifications.pdf.

Tercan, S.H., Eid, B., Heidenreich, M., Kogler, K., Akyurek, O., 2021. Financial and technical analyses of solar boats as a means of sustainable transportation. Sustain. Prod. Consump. 25, 404–412. http://dx.doi.org/10.1016/j.spc.2020.11.014.

Wang, H., Boulougouris, E., Theotokatos, G., Zhou, P., Priftis, A., Shi, G., 2021. Life cycle analysis and cost assessment of a battery powered ferry. Ocean Eng. 241, http://dx.doi.org/10.1016/j.oceaneng.2021.110029.

Wave Dragon, 2022.http://www.wavedragon.net.

Wave dragon 1.5 MW, 2015. Wave dragon. https://energiforskning.dk/sites/energiforskning.dk/files/slutrapporter/wd15mwv4_efm-17.pdf.

Worldbank, 2022a. Real interest rate (%) - Hong Kong SAR, China. https://data.worldbank.org/indicator/FR.INR.RINR?end=2019&locations=HK&start=2010&view=chart.

Worldbank, 2022b. Official exchange rate (LCU per US$, period average) - Hong Kong SAR, China. The World Bank. https://data.worldbank.org/indicator/PA.NUS.FCRF?end=2019&locations=HK&start=2011.

Xu, X., Hu, W., Liu, W., Du, Y., Huang, R., Huang, Q., Chen, Z., 2021. Risk management strategy for a renewable power supply system in commercial buildings considering thermal comfort and stochastic electric vehicle behaviors. Energy Convers. Manage. 230, http://dx.doi.org/10.1016/j.enconman.2021.113831.

Yan, J., Zhang, J., Liu, Y., Lv, G., Han, S., Alfonzo, I.E.G., 2020. EV charging load simulation and forecasting considering traffic jam and weather to support the integration of renewables and EVs. Renew. Energy 159, 623–641. http://dx.doi.org/10.1016/j.renene.2020.03.175.

Yu Wang, L.L., Wennersten, Ronald, Sun, Qie, 2019. Peak shaving and valley filling potential of energy management system in high-rise residential building. https://www.sciencedirect.com/science/article/pii/S1876610219305107.

Zandrazavi, S.F., Guzman, C.P., Pozos, A.T., Quiros-Tortos, J., Franco, J.F., 2022. Stochastic multi-objective optimal energy management of grid-connected unbalanced microgrids with renewable energy generation and plug-in electric vehicles. Energy 241, http://dx.doi.org/10.1016/j.energy.2021.122884.

Zhan, K., Hu, Z., Song, Y., Lu, N., Xu, Z., Jia, L., 2015. A probability transition matrix based decentralized electric vehicle charging method for load valley filling. Electr. Power Syst. Res. 125, 1–7. http://dx.doi.org/10.1016/j.epsr.2015.03.013.

Zhang, K., Xu, L., Ouyang, M., Wang, H., Lu, L., Li, J., Li, Z., 2014. Optimal decentralized valley-filling charging strategy for electric vehicles. Energy Convers. Manage. 78, 537–550. http://dx.doi.org/10.1016/j.enconman.2013.11.011.

Zhou, Y., Cao, S., 2020. Quantification of energy flexibility of residential net-zero-energy buildings involved with dynamic operations of hybrid energy storages and diversified energy conversion strategies. Sustain. Energy Grids Netw. 21, http://dx.doi.org/10.1016/j.segan.2020.100304.

Zhou, S., Cao, S., Wang, S., 2022. Realisation of a coastal zero-emission office building with the support of hybrid ocean thermal, floating photovoltaics, and tidal stream generators. Energy Convers. Manage. 253, http://dx.doi.org/10.1016/j.enconman.2021.115135.